Realistic estimation for the detectability of dark matter subhalos using Fermi-LAT catalogs

Francesca Calore, Valentina De Romeri, Mattia Di Mauro, Fiorenza Donato, and Federico Marinacci

Phys. Rev. D **96**, 063009 — Published 15 September 2017

DOI: 10.1103/PhysRevD.96.063009

LAPTH-064/16, IFT-UAM/CSIC-16-118, FTUAM-16-40

Realistic estimation for the detectability of dark matter sub-halos with *Fermi*-LAT

Francesca Calore,[1,*] Valentina De Romeri,[2,†] Mattia Di Mauro,[3,‡] Fiorenza Donato,[4,§] and Federico Marinacci[5,¶]

[1] *LAPTh, CNRS, 9 Chemin de Bellevue, B.P. 110 Annecy-le-Vieux, F-74941, France*
[2] *Departamento de Física Teórica and Instituto de Física Teórica, IFT-UAM/CSIC, Universidad Autónoma de Madrid, Cantoblanco, 28049 Madrid, Spain*
[3] *W. W. Hansen Experimental Physics Laboratory, Kavli Institute for Particle Astrophysics and Cosmology, Department of Physics and SLAC National Accelerator Laboratory, Stanford University, Stanford, CA 94305, USA*
[4] *Dipartimento di Fisica, Università di Torino and Istituto Nazionale di Fisica Nucleare, Sezione di Torino, via P. Giuria 1, I-10125 Torino, Italy*
[5] *Kavli Institute for Astrophysics and Space Research, Massachusetts Institute of Technology, Cambridge, MA 02139, USA*

Numerical simulations of structure formation have recorded a remarkable progress in the recent years, in particular due to the inclusion of baryonic physics evolving with the dark matter component. We generate Monte Carlo realizations of the dark matter sub-halo population based on the results of the recent hydrodynamical simulation suite of Milky Way-sized galaxies [1]. We then simulate the gamma-ray sky for both the setup of the 3FGL and 2FHL *Fermi* Large Area Telescope (LAT) catalogs, including the contribution from the annihilation of dark matter in the sub-halos. We find that the flux sensitivity threshold strongly depends on the particle dark matter mass, and more mildly also on its annihilation channel and the observation latitude. The results differ for the 3FGL and 2FHL catalogs, given their different energy thresholds. We also predict that the number of dark matter sub-halos among the unassociated sources is very small. A null number of detectable sub-halos in the *Fermi*-LAT 3FGL catalog would imply upper limits on the dark matter annihilation cross section into $b\bar{b}$ of $2 \cdot 10^{-26}$ $(5 \cdot 10^{-25})$ cm^3/s with $M_{\rm DM}$= 50 (1000) GeV. We find less than one extended sub-halo in the *Fermi*-LAT 3FGL catalog. As a matter of fact, the differences in the spatial and mass distribution of sub-halos between hydrodynamic and dark matter-only runs do not have significant impact on the detectability of dark sub-halos in gamma rays.

* francesca.calore@lapth.cnrs.fr
† valentina.deromeri@uam.es
‡ mdimauro@slac.stanford.edu
§ donato@to.infn.it
¶ fmarinac@mit.edu

I. INTRODUCTION

One of the most intriguing mysteries in modern physics is that about 85% of all matter in the Universe is of unknown origin [2]. Despite the extraordinary achievements in measuring the gravitational effect of this missing component, called dark matter (DM), still no direct evidence of its particle nature has been verified. One of the most well-motivated classes of DM particle candidates is represented by Weakly Interacting Massive Particles (WIMPs) (see for instance refs. [3, 4] for a review). WIMPs can naturally achieve the correct relic DM abundance through self-annihilation in the early Universe, and can be searched for with several techniques. Besides direct DM detection experiments and searches at colliders, indirect DM searches aim to detect the fluxes of stable particles produced by DM annihilation or decay processes. Among the possible final products of DM interactions, gamma rays are one of the most promising channels for DM detection, since they preserve the spectral and spatial features of the prompt DM signal.

Recent years have witnessed a steady progress in the field of DM indirect detection through gamma rays. In particular, the Large Area Telescope (LAT), aboard the *Fermi* satellite, is currently one of the most sensitive instruments collecting gamma rays from the whole sky. The *Fermi*-LAT Collaboration and other groups have already set severe constraints on the WIMP DM parameter space with searches towards dwarf spheroidal galaxies [5], of gamma-ray lines [6, 7], in the diffuse Galactic and extragalactic emission [8–10], galaxy clusters [11] and the Galactic Centre [12, 13].

It is well known that the sensitivity to DM detection in a specific target depends crucially on the distribution of DM in that particular environment. In the context of the concordance ΛCDM cosmology [2, 14], a firm theoretical prediction is that structures in the Universe form in a hierarchical way. DM, interacting through gravity, collapses into structures known as DM halos [15, 16], which assemble in a bottom-up way from the least massive, gradually merging to create larger systems [17]. These theoretical predictions are confirmed by numerical simulations of structure formation modeling the gravitational interaction of the DM component in a full cosmological set-up (also known as DM only or N-body simulations), which have been widely successful at reproducing the large-scale distribution of structures in the Universe [18–20].

On smaller scales, i.e. within individual DM halos, the results obtained from numerical simulations are more uncertain. At those scales baryon physical processes, that give origin to the present-day galaxy population, and that might also have a substantial effect on the DM distribution in halos [21–23] and its detection, are at play. A complete understanding of galaxy formation and evolution would require simulating these physical processes from first principles, but this turns out to be an incredibly challenging task given the extreme dynamic range of scales that has to be resolved. Notwithstanding these difficulties – and the inevitable limitations they entail to a fully predictive theory of galaxy formation – remarkable progress has been accomplished in the field over the last years. Hydrodynamical simulations of galaxy formation are now able to produce a galaxy population whose properties are in broad agreement with the observational constraints [24–26]. Moreover, the goal of forming a disc galaxy like our own Milky Way (MW), which for decades has been one of the most intricate problems in the context of ΛCDM cosmological simulations, seems now to be achieved by many groups using different numerical techniques [1, 27–34].

A robust prediction of cosmological simulations (with or without the inclusion of baryons) is that DM halos are populated by smaller substructures, usually referred to as sub-halos (SHs). The largest sample of galactic SH population include dwarf galaxies, which typically contain a modest amount of baryonic matter, i.e. gas and stars. However, dwarfs are only the small "visible" portion of a larger population of DM SHs which lack any significant baryonic content and are therefore not detectable in the optical wavelength. Besides the objects that are too faint to be in the reach of current optical surveys such as the Dark Energy Survey (DES) [35–37], there might exist a number of totally dark SHs that do not contain any star or gas. At present, the number of dwarf galaxies discovered in the Local Group is about 30 [5, 36, 38, 39]. As DM dominated structures, SHs could emit gamma rays created by WIMPs self-annihilation and they may be detected as individual sources in the sky, depending on the signal intensity and on the astrophysical background along the line of sight. On top of that, SHs that are too faint to be detected as individual sources would instead contribute to the diffuse gamma-ray emission [40] and signatures for this unresolved population of SHs might be looked for in the gamma-ray diffuse background intensity, e.g. [41, 42], and/or small scale gamma-ray anisotropies, e.g. [43, 44].

The *Fermi*-LAT Collaboration recently released the third catalog of point sources (3FGL) [45] that contains sources detected after four years of operation in the energy range 0.1 – 300 GeV with Pass 7 data. The 3FGL catalog contains about 3000 sources, where the large majority of detected objects at a latitude $|b| > 20^\circ$ are extragalactic Active Galactic Nuclei (AGN). *Fermi*-LAT also recently released a new event-level analysis, Pass 8, that increases significantly the acceptance of the telescope and, at the same time, improves its angular resolution [46]. Exploiting these improvements, the *Fermi*-LAT Collaboration has compiled and released the second catalog of hard *Fermi*-LAT sources (2FHL) [47]. This catalog fills the energetic data gap with current atmospheric Cherenkov telescopes and contains about 360 sources detected with 80 months of exposure time and between 50 – 2000 GeV.

In both catalogs, a large fraction of sources remain unassociated: about 15% in the 2FHL and 30% in the 3FGL. The probabilistic association of sources made by *Fermi*-LAT takes into account the density of sources in the region around the gamma-ray source and its distance to close-by objects detected in other wavelengths[1]. Hence, unassociated sources are point-like gamma-ray emitters detected as such by the LAT, but lacking association with astrophysical objects known in other wavelengths. Interestingly, the sample of unassociated sources in the *Fermi*-LAT catalogs might already contain gamma-ray emitting DM SHs. Their identification requires the determination of a realistic sensitivity flux threshold to the specific detection of DM SHs, which is lacking in the current literature and is one of the primary goals of the present work.

We analyze the detectability of DM SHs in current *Fermi*-LAT catalogs. Previous works have already addressed this issue [48–51], examining the 3FGL source catalog and modeling the DM SHs distribution in a MW like galaxy, based on the N-body simulation Via Lactea II [52]. The authors of [48] identified 24 3FGL bright sources that may be consistent with DM (with mass about $\sim 20 - 70$ GeV) annihilation in Galactic SHs, as well as with faint gamma-ray pulsars. In [49] they further scrutinized the source 3FGL J2212.5+0703 from the previous subset, as a possible DM SH and gave also a plausible alternative astrophysical explanation. Both works set constraints on the DM annihilation cross section. Ref. [50] updates the prior studies predicting a smaller number (at most $\sim$10) of SHs which could possibly be detected by the *Fermi*-LAT as unassociated sources. More recently, ref. [53] revisited the previous analyses focusing on the prospects of detecting DM SHs with the future Cherenkov Telescope Array observatory [54]. Using machine learning classifiers, ref. [55] recently looked for novel source classes in the sample of 3FGL unassociated sources. They found 34 potential candidates and placed upper limits on the number of Galactic SHs and, correspondingly, on the DM annihilation cross section. Finally, the authors of [51] revisited the constraints on the DM annihilation cross section inferred from searches for SHs candidates among the *Fermi*-LAT 3FGL unassociated sources. They consider the cosmological N-body simulations Via Lactea II [52] and ELVIS [56] to model the local dark matter SH population. Their placed limits on the DM annihilation cross section are slightly weaker than those from dwarfs while being stronger than those found by ref. [50]. Our work further improves the antecedent studies with an array of novelties:

- The prediction of the DM SHs gamma-ray signal is based on one of the most recent cosmological numerical simulations that includes baryonic physics [1, 57]. For the first time, we model the signal as expected in both hydrodynamic and DM only simulations of the MW and we compare the results, quantifying possible differences.
- The setups of both 3FGL and 2FHL *Fermi*-LAT catalogs are simulated to derive the sensitivity of the LAT to DM SHs detection, the advantage being a wider DM mass coverage.
- Instead of using a fixed flux detection threshold, as usually done, we provide a realistic estimation for the sensitivity of the LAT to the DM flux from SHs at high-latitude as a function of DM annihilation channel, DM mass and SH Galactic latitude. We show that the accurate determination of the sensitivity to DM spectra leads to significant differences with respect to a fixed flux threshold.
- We estimate the detectability of extended DM SHs comparing the extension of gamma-ray emission from DM interaction with the minimum extension detected in the 3FGL catalog, by adopting a more conservative approach than ref. [51].

We focus on the detectability of SHs as individual point sources in *Fermi*-LAT catalogs (i) for improving on previous works on this topic as explained above, and (ii) for providing robust predictions which do not require critical extrapolations beyond the simulation's resolution limits (in mass and space), but rely only on simulation data instead. Indeed, as we will see in what follows, the brightest SHs are, in general, the most massive ones. As such, our predictions of the number of detectable SHs as individual sources depend only on the simulation data. On the other hand, determining the distribution and luminosity function of lower-mass SHs, the majority of which will remain undetectable as single point sources and could contribute to the diffuse gamma-ray background [41], would rely on extrapolations of the simulation's results beyond its mass resolution limit. This extrapolation procedure is the main theoretical uncertainty that affects the predictions at small scales [58], and we do not tackle this issue down to the smallest SHs masses in the present work. We also remind that faint (i.e. unresolved by the LAT) extragalactic sources such as blazars or Radio Galaxies are predicted to give a large contribution to the diffuse gamma-ray background (see e.g. [59, 60]). Nevertheless, we will discuss the effect that adding lower-mass SHs has on our predictions.

The paper is structured as follows. In Sec. II, we describe how we model the DM SHs distribution – quantifying the discrepancies between the hydrodynamic scenario and the pure DM one – and their annihilation flux into gamma rays. In Sec. III we derive the *Fermi*-LAT sensitivity to DM spectra in the 3FGL and 2FHL catalogs setups. In

[1] Association using only gamma rays is possible only for pulsars, for which the LAT could detect the gamma-ray pulsation and thus classify it as a pulsar. However, this kind of association is extremely rare.

Sec. IV we present implications for DM phenomenology, namely the number of detectable SHs, constraints on the DM annihilation cross section, and source count distribution. In Sec. V we discuss the possibility of resolving the extension of the detectable SHs. Finally, in Sec. VI we summarize our conclusions.

II. DARK MATTER IN THE GALAXY AND GAMMA-RAY SIGNALS

For modeling the SH population in the Galaxy, we use the results of two cosmological simulations of a MW-size halo [57]. The first simulation is the full hydrodynamic run Aq-C-4 in [1] ("Hydro" run hereafter), while the second one is a control DM-only simulation of the same halo (from now on, the DMO run) [57]. Both these simulations use the initial conditions of the halo C of Aquarius Project [61] (hereafter AQ08) at resolution level 4 (see table I for details). While the DMO simulation models only gravitational interactions of the DM component, the Hydro case is equipped with a comprehensive galaxy formation physics model largely based on the Illustris simulation [1, 24]. This model includes the most important physical processes for galaxy formation and its main constituents are: (i) a module for radiative cooling of the gas; (ii) a subgrid description of the interstellar medium and star formation out of the dense gas ($n \sim 0.1\,\mathrm{cm}^{-3}$) following the prescriptions of [62], modified for a Chabrier [63] initial mass function; (iii) routines following stellar evolution and in particular tracking mass and metal return from type II, type Ia supernovae and AGB stars to the interstellar medium; (iv) stellar feedback in the form of galactic winds following a kinetic implementation in which the wind velocity is scaled to the size of the underlying DM halo; and (v) modules for supermassive black hole seeding, accretion, merging and the associated AGN feedback. For reason of space we do not enter into the detail of the galaxy formation physics implementation here, but refer the reader instead to refs. [1, 29, 64] for a full description. Both runs are performed with the moving-mesh code Arepo [65], a highly versatile code for cosmological simulations that models the hydrodynamics via a finite volume technique on an unstructured Voronoi mesh. This mesh is allowed to move with the gas, thus adapting to the flow characteristic and giving rise to a manifestly Galilean-invariant method that combines the strengths of both Lagrangian and Eulerian approaches yielding superior results in terms of accuracy. The evolution of the two simulated halos is followed from very high redshift ($z = 127$) down to redshift zero.

We model the SH distribution in the halo in two steps: First, we analyze the results of the Hydro and DMO simulations and we derive analytic parameterizations of the SH spatial and mass distributions. Secondly, using the analytic prescriptions for the statistical distribution of SH position and mass, we generate a mock population of Galactic SHs in multiple Monte Carlo realizations. In this section we describe these two steps in more detail.

A. Modeling the dark matter distribution in the Galaxy

We consider the distribution of SHs as predicted by simulations of galaxy formation that include the effect of baryons in the galaxy evolution process. There exist three main processes driven by baryonic physics: adiabatic contraction, tidal disruption and reionization, which act jointly to shape the DM distribution in both the host halo and in its SHs. The effects of these processes are respectively of: (i) increasing the density in the center of the Galaxy, (ii) removing both DM and luminous matter and redistribute them in the SHs and (iii) evaporating the gas and preventing gas accretion from the intergalactic medium. As a result of the baryonic actions, usually one finds fewer SHs in the Hydro simulations than in the DMO ones. In particular, fewer low-mass SHs are generated in the Hydro case [57]. Typically, there are also differences in the abundance and spatial distribution of the SHs, especially in the central region of the main halo. Such a depletion is caused by (a) gravitational shocks as SHs pass in the vicinity of the disk [e.g. 66, 67] and (b) the contracted DM distribution generated by the cooling of baryons at the center of the halo [e.g. 68–70] As a consequence of these processes, tidal disruption is enhanced and SHs are disrupted more often, up to a factor of two, in the center [71, 72].

The two simulations under study model the formation of a $2.04 \times 10^{12}\ M_\odot$ and a $1.77 \times 10^{12}\ M_\odot$ halo, in the DMO and Hydro case respectively, and of their substructures. The typical parameters of the two simulations are summarized in Tab. I. To identify the SHs we used the Amiga halo finder [73, 74], a density-based algorithm which determines prospective SHs centers with the use of a hierarchy of adaptive grids that are also employed to collect the particles potentially associated to any given center. The final structures are then found by iteratively removing gravitationally unbound particles, assuming spherical symmetry, from the potential candidates identified in the previous step. We stress that this procedure is applied in the Hydro case to find all SHs of the main halo *regardless* of their stellar content. SHs identified in the Hydro simulation can be either dark or luminous, and thus be identified as dwarf satellite galaxies. Whether or not a SH is able to form stars depends on its mass, having that low-mass SHs are likely to be dark, while at the high-mass end they tend to host a stellar component. The mass range for which this transition occurs is $\sim 10^{7-8}\,\mathrm{M}_\odot$ [57].

Run	$R_{\rm vir}$ (kpc)	$M_{\rm tot}$ ($10^{12}\ M_\odot$)	$m_{\rm gas}$ ($10^5\ M_\odot$)	$m_{\rm DM}$ ($10^5\ M_\odot$)	ϵ (pc)
DMO	326	2.04	-	3.2	340
Hydro	311	1.77	0.5	2.7	340

TABLE I. Characteristic parameters of the two (DMO and Hydro) simulation runs at $z = 0$. The virial radius $R_{\rm vir}$ is defined as a sphere enclosing an over-density of 178 with respect to the critical density. $M_{\rm tot}$ is the total mass included inside $R_{\rm vir}$; $m_{\rm gas}$ and $m_{\rm DM}$ are the mass resolution of gas and DM, respectively. Finally, ϵ is the gravitational softening length of the DM particles. For gas cells the softening length is adaptive and scaled proportionally to their sizes. Its minimum physical value is the same as the one used for DM particles.

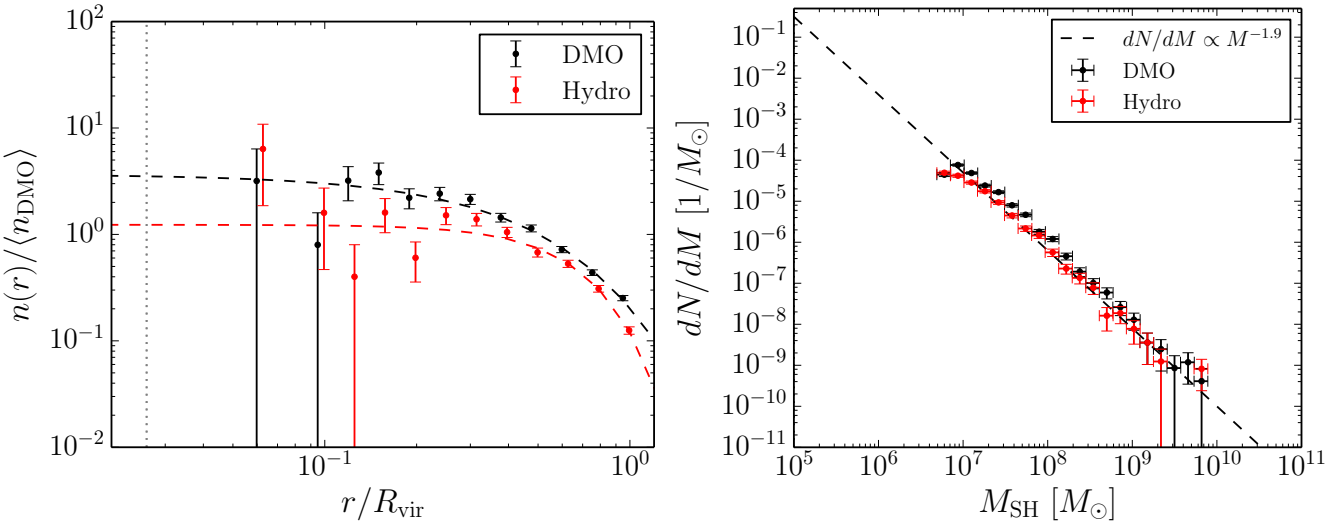

FIG. 1. *Left panel*: Spatial distribution $n(r)$ of SHs in the Hydro (red points) and DMO (black points) runs [57], normalized to the total number of SHs in the DMO run. The dashed red (black) line is the best fit for an Einasto parameterization of the spatial profile, see Eq. (1). The dotted vertical line indicates the position of the Sun for the DMO run. *Right panel*: SH differential mass abundance dN/dM in the Hydro (red points) and DMO (black points) run. The lower limit of the mass axis corresponds to the smallest SH mass in AQ08 ($M_{\rm SH}^{\rm min} = 10^5\ M_\odot$). Overlaid (dashed black curve) is the mass distribution function that best fits the AQ08 results [61].

In order to avoid resolution effects, which may affect the properties of the SHs identified in the simulations and, consequently, our analysis, we apply two cuts to the sample of SHs identified by the halo finder. First, we consider SHs formed by at least 20 particles. Second, we adopt a restriction on the SHs minimum value of the maximum rotational velocity, $v_{\rm max}$. In both runs we require that $v_{\rm max} \gtrsim \sqrt{(M(<r_{\rm max})\,G/(2.8\,\epsilon)} \gtrsim 4$ km/s, where G is the universal gravitational constant $G = 4.3 \times 10^{-3}$ pc $M_\odot{}^{-1}$(km/s)^2 and ϵ is the gravitational softening length; $r_{\rm max}$ is defined as the radius at which $v_{\rm max}$ is reached. As a result, the DMO (Hydro) run provides a reliable subsample of ~ 1200 (800) SHs with masses $M_{\rm SH} \gtrsim m_{\rm DM} \times 20 \sim 5.4 \times 10^6\ M_\odot$. Typically, discrepancies between hydrodynamic and DMO runs are expected for halos with masses larger than $10^6 - 10^7\ M_\odot$, where stars can form, as also found in ref. [57]. However, while studying the impact of hydrodynamics in the mass and spatial distribution of Galactic SHs, we will also discuss the effect of lower-mass SHs (see section IV).

SH spatial distribution. From the simulations' data, we analyze the spatial distribution of SHs in the Galaxy and perform a fit to the radial number density of SHs $n(r)$ for both the DMO and Hydro runs with an Einasto function [75]:

$$n(r)/\langle n\rangle_{\rm DMO} = n_{-2} \exp\left\{ -\frac{2}{\alpha}\left[\left(\frac{r}{r_{-2}}\right)^{\alpha} - 1\right]\right\}. \quad (1)$$

Here r is the distance from the galactic center, $n(r)$ is normalized to the total number $\langle n\rangle_{\rm DMO}$ of SHs in the DMO run (in analogy with ref. [57]). The free parameters in the fit are n_{-2}, α, and r_{-2}. The best-fit values that we find by minimising the χ^2 are: $n_{-2} = 0.66 \pm 0.06$ $(0.50 \pm 0.0.03)$, $\alpha = 1.17 \pm 0.15$ (2.20 ± 0.29) and the scale radius $r_{-2} = 0.64 \pm 0.02$ (0.65 ± 0.02) $R_{\rm vir}$ in the DMO (Hydro) simulation, respectively. We show in Fig. 1 (left panel) the result of the fit to $n(r)$ for the DMO and Hydro runs. The distance r is normalized to the virial radius of the main

halo[2] ($R_{\rm vir}^{\rm DMO} = 326$ kpc and $R_{\rm vir}^{\rm Hydro} = 311$ kpc). As already shown in [57], the radial number density of SHs in the Hydro run is consistently lower than in the DMO one, thus meaning that the SHs are being disrupted more often in the Hydro simulation.

SH mass distribution. Most of numerical simulations in the literature (including AQ08 [61]) have shown that the SH differential mass abundance is well described by a power law $dN/dM \sim M^{-\alpha_M}$, whose slope is slightly shallower than -2, over many decades in mass. In Fig. 1 (right panel) we show the number of SHs per unit mass interval, where the slope of the SH mass distribution for both the DMO and Hydro runs are the same and consistent with AQ08 results, having $\alpha_M = 1.9$ [57].

DM distribution and density profile of the SHs. The gamma-ray emissivity from DM annihilation in SHs is determined by the internal spatial profile of the DM SH. Contrary to the main halo, whose DM density profile has been demonstrated to differ significantly in DMO and Hydro runs [21, 57, 76, 77], in the simulations considered here the SH DM density profiles in the Hydro simulation are compatible with their counterparts in the DMO run above the simulation resolution [57]. In particular, no dark matter cores are formed. We note that a conclusive agreement on this aspect is still lacking [22, 78, 79], and that cores might be formed or not for the same initial conditions even depending on the way the weighting in distributing supernova energy to the gas is performed [78]. We stress however that those discrepancies apply mostly to high mass SHs ($M \gtrsim 10^9\, M_\odot$), where supernova energy is enough to drive the dark matter profile transformation [e.g. 22, 80]. Indeed, at a scale of $10^8\, M_\odot$ and below, baryonic effects are likely not to play a significant role in altering the shape of DM halos, given the very low conversion efficiency of gas into stars. We note that, for studying the detectability of DM SHs in gamma rays, we are interested in the integral over the SH's volume of its gamma-ray emissivity. Therefore, differences between cored and cuspy density profiles in the inner part of the object are less dramatic when considering the whole SH extension. Since a conclusive evidence on the effect of baryons at different mass scales has not been reached yet, we here make the assumption that the radial DM density profile of the SHs is described by the Einasto parametrization [81]:

$$\rho(r) = \rho_s \exp\left\{ -\frac{2}{\alpha_\rho}\left[\left(\frac{r}{r_s}\right)^{\alpha_\rho} - 1\right]\right\}, \tag{2}$$

where r is the distance from the center of the SH. We fix $\alpha_\rho = 0.16$, in agreement with what was found in AQ08. Therefore, the SHs density profile is described by a function with two free parameters: the specific density ρ_s and the scale radius r_s, defined at the point where $\rho(r)$ has a slope close to a power law with index -2. Given the mass of the SHs and r_s, ρ_s is fully determined. On the other hand, r_s has to be determined from the simulation results. Assuming that the density distribution of DM within each SH follows an Einasto profile, there are two quantities which are sufficient to determine the density profile uniquely: the mass of the SH (or equivalently $v_{\rm max}$) and $r_{\rm max} = 2.189\, r_s$ [61].

From the simulation data, we find that the values of $r_{\rm max}$ are correlated with the SH mass. We perform a fit to the $r_{\rm max}$ data as a function of $M_{\rm SH}$ with a polynomial function. We derive the best-fit parameterization to be in the form:

$$\begin{aligned} &\log_{10}(r_{\rm max}/{\rm kpc}) = \\ &a + b\, \log_{10}(M_{\rm SH}/{\rm M}_\odot) + c\, (\log_{10}(M_{\rm SH}/{\rm M}_\odot))^2 \end{aligned} \tag{3}$$

with best-fit parameters[3]: $a = -5.384$, $b = 1.156$, $c = -0.056$ for the Hydro run. The standard deviation of the data around the best-fit value is $\sigma = 0.145$. In Fig. 2 we show $r_{\rm max}$ as a function of the SH mass from the DMO and Hydro runs. We overlay the corresponding best-fit relation $r_{\rm max}$ – $M_{\rm SH}$ for the Hydro case. By comparing the values of $r_{\rm max}$ for the Hydro and DMO case, we can see that the impact of baryonic physics on the scale radius of the SHs is actually mild: the values of $r_{\rm max}$ in the Hydro case are quite similar to their DMO counterparts. In general, given a $M_{\rm SH}$, r_s tends to be only slightly smaller in the DMO case.

We emphasize that the polynomial fit can be considered reliable in the parameter range tested by the simulation, that is $5 \times 10^6 \lesssim M_{\rm SH} \lesssim 10^{10}\, M_\odot$. Its extrapolation, especially at larger masses, may be affected by sizeable statistical uncertainties. We note that assuming, for example, a linear distribution of $r_{\rm max}$, implies that at a given $M_{\rm SH}$ the $r_{\rm max}$ is larger, and hence the scale radius r_s is also larger, thus leading to different results for the DM annihilation signal.

Indeed the scale radius, $r_s = r_{\rm max}/2.189$, which is closely correlated to the SH mass accretion history, affects the computation of the astrophysical factor (see Eq. (7)) appearing in the DM gamma-ray flux: smaller r_s correspond to denser halos (see Eq. (2)).

---

[2] $\Delta_{\rm vir}(z) = 178$ is the adopted virial over-density.

[3] To optimize the fit, we have removed the few isolated points with masses $M_{\rm SH} \gtrsim 5 \times 10^9\, M_\odot$.

Concentration. A very useful parameter that can be introduced to describe the internal DM halos structure is the *concentration*. This quantity and its different parameterizations (in terms of SH mass, circular velocity and radial distance) have been widely analyzed in the literature, e.g. [52, 82–85]. In full generality, the concentration parameter c is defined as the mean over-density within the radius of the peak circular velocity $r_{\rm max}$ in units of the critical density of the Universe at present ($\rho_{cr} = 147.897\ M_\odot/{\rm kpc}^3$):

$$c = \frac{\bar{\rho}(r_{\rm max})}{\rho_{cr}} = 2\left(\frac{v_{\rm max}}{H_0\, r_{\rm max}}\right)^2 , \tag{4}$$

where $H_0 = 73$ km s^{-1}Mpc^{-1} is the Hubble constant. Equivalently, the concentration parameter can be cast as the ratio between the virial radius (the radius which encloses an average DM density $\sim 200 \times \rho_{cr}$) and the scale radius:

$$c = \frac{r_{\rm vir}}{r_s}. \tag{5}$$

SHs are in general more concentrated than field halos of the same mass, due to the tidal force that removes material from their outer regions, see e.g. [86]. It has also been shown that the SH concentration depends on the mass of the SH and on its distance from the center of the main halo [52, 82, 85]. While a detailed analysis of the concentration is beyond the scope of this paper, different concentration parameterizations depending on the SH mass and the distance have been proposed [52, 82, 85], for both main halos and SHs. Nevertheless, in the present work we will not use any analytical parameterization of the concentration which, having been derived for other simulation results, might bias our results. Instead, we directly use the output data of the simulation – namely the distribution of $r_{\rm max}$ – to model the scale radius. As described below, we will take into account the mass dependence of $r_{\rm max}$, which is somewhat related to the mass dependence of the concentration parameter, although by means of a quantity directly output by the simulation. Yet, we do not include any radial dependence of $r_{\rm max}$ in our modelling. We will comment about the impact on the predicted flux below. ~~The advantage of this choice is to avoid making any a-priori assumption on the DM distribution inside the SHs and rather to model their distribution as it comes out from the numerical simulation.~~

Monte Carlo simulation. Based on the modeling outlined above and derived by analyzing the simulations' data, we generate 100 Monte Carlo realizations of the SHs population in a MW-like Galaxy, for both the DMO and Hydro cases. The number of simulated SHs in each realization is consistent with the total DM mass in the original numerical simulation [57]. In total, we generate about 800 (1200) SHs in each Hydro (DMO) Monte Carlo realization.

For each SH, we randomly extract its position in the Galaxy and its mass from the spatial and mass distributions outlined above. We also include the uncertainty on the best-fit parameters of the distributions, in order to account for the the halo-to-halo variation more realistically, i.e. the variation that would be present if we had disposed of more than one main host halo. The viral radius of each SH is defined as the tidal radius of the SH, modeled according to Eq. (12) of AQ08, and dependent on the SH position and mass.

In the Monte Carlo simulation, given the SH mass, we compute the value of $r_{\rm max}$ from the polynomial best-fit and we add a 3σ log-normal dispersion about the best-fit relation in Fig. 2. We then get the value of $r_s = r_{\rm max}/2.189$ [61].

B. Dark matter annihilation gamma-ray signatures

DM particle annihilation produces gamma rays through direct emission, the so-called prompt mechanism, and through indirect processes, such as the Inverse Compton scattering of final electrons and positrons with low-energy ambient photons, or bremsstrahlung of the same population of electrons and positrons with the interstellar gas. Usually different primary annihilation channels are studied assuming a branching ratio of 100% in each channel separately. Here, we take into account one typical hadronic annihilation channel, $b\bar{b}$, and the leptonic channel that gives the largest DM gamma-ray flux, i.e. $\tau^+\tau^-$. For both pairs, the most important gamma-ray emission mechanism is the prompt one [8, 87]. We therefore do not include any secondary emission in this analysis.

The flux of photons, F, integrated over the energy range $\Delta E = E_1 - E_0$ from a given region of the sky and produced by the annihilation of self-conjugated DM particles is calculated as:

$$F_{[E_1,E_0]} = \frac{\langle\sigma v\rangle}{8\pi M_{\rm DM}^2}\, \mathcal{I}_{[E_1,E_0]}\, \mathcal{J}, \tag{6}$$

where $M_{\rm DM}$ is the DM particle mass, $\langle\sigma v\rangle$ is the thermal averaged annihilation cross section, $\mathcal{I}_{[E_1,E_0]}$ is the integrated energy spectrum $\mathcal{I}_{[E_1,E_0]} = \int_{E_0}^{E_1} dN_{\rm DM}/dE\ dE$ in the energy range $[E_0, E_1]$. The energy spectra of gamma rays

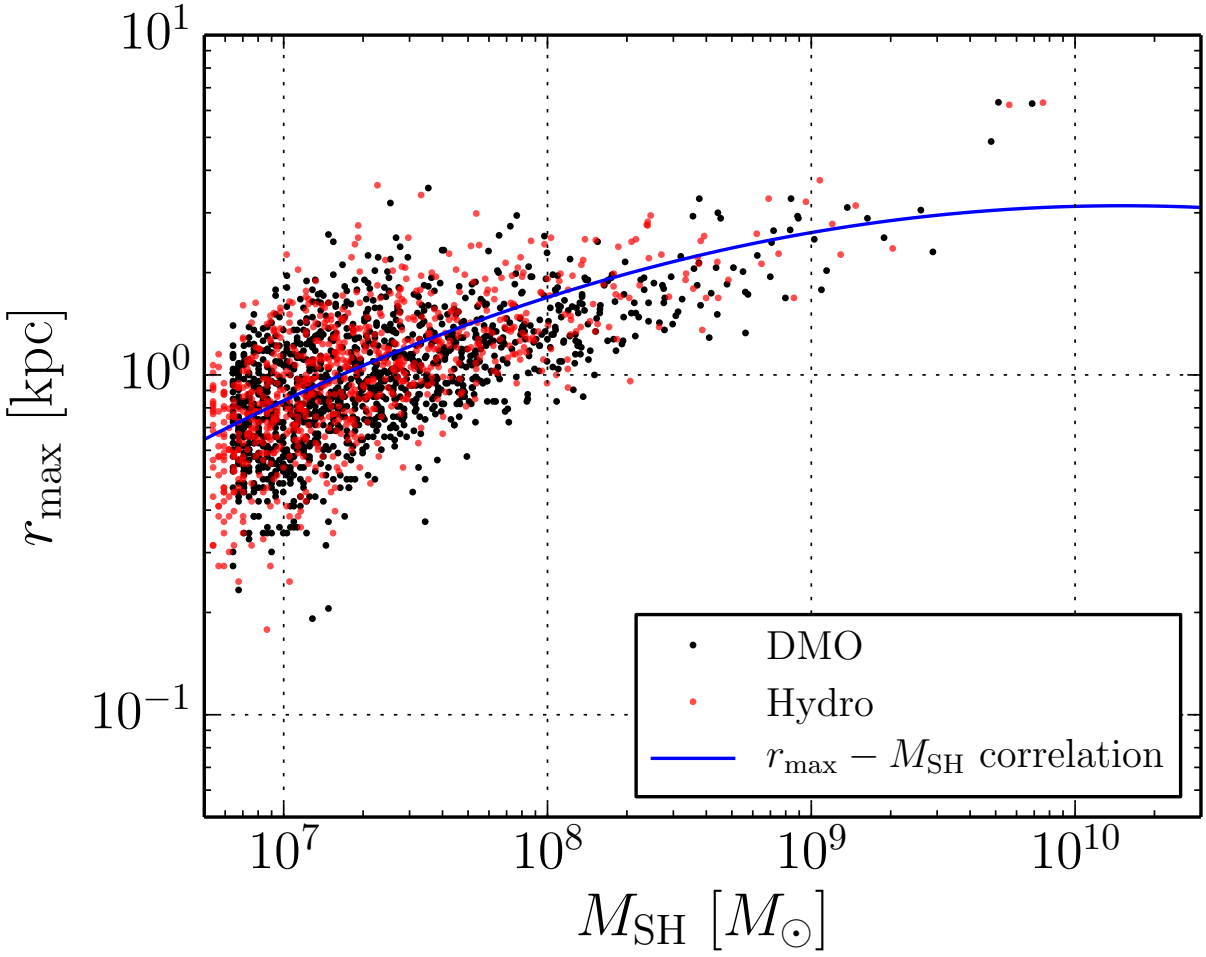

FIG. 2. $r_{\rm max}$ as a function of the SH mass, $M_{\rm SH}$ for the Hydro (red) and DMO (black) simulation runs. Overlaid, in blue, the best-fit relation for the Hydro run as in eq. (3).

produced from DM annihilation in $b\bar{b}$ and $\tau^+\tau^-$ channels are taken from [87], where they are calculated using PYTHIA 8 [88] event generator. Finally, $\mathcal{J}$ is the geometrical factor defined as:

$$\mathcal{J} = 2\pi \int_{\theta_{\rm min}}^{\theta_{\rm max}} d\theta \sin(\theta) \int_{\rm l.o.s} \rho^2(r(l,\theta)) dl, \tag{7}$$

where θ is the opening angle with respect to the line of sight l that points to the center of the SH; $\theta_{\rm min}$ is set to 0 and thus corresponds to the direction of the SH center, while $\theta_{\rm max}$ is π. The radial distance r from the center of the SH is defined as $r^2 = d^2 + l^2 - 2\,l\,d\,\cos(\theta)$.

The $\mathcal{J}$-factor encodes the information about the geometry of the emission and it is a direct measure of the intensity of the signal, being $F_{[E_1,E_0]} \propto \mathcal{J}$. We compute the $\mathcal{J}$-factor for the two sets of SHs in our Monte Carlo simulations. In Fig. 3 we show the values of the $\mathcal{J}$-factor versus the SH mass for the Hydro case. The color code indicates the distance of the SH from Earth (in kpc), assuming the Sun distance from the Galactic center to be 8.5 kpc – blue being the solutions for the closest SHs and red those for the farthest ones. We have proven that the results for the Hydro and DMO cases are fully comparable, as it can already been deduced from Fig. 2. Given the mild difference between the Hydro and the DMO cases, in the following we will show results only for the Hydro case. We also have numerically checked that assuming the extremely cored Burkert profile [89] for the more massive SHs ($M \gtrsim 10^8\,M_\odot$) at different distances from the galactic center leads to a difference of a factor of at most two in the $\mathcal{J}$-factor. We have checked that neglecting the radial dependence of the concentration on the distance of the SH from the Galactic center will give at most a variation of less than a factor of four – by assuming the radial dependence of Ref. [85] – for SHs closest to the Galactic center, regardless of their mass. Finally, we would like to note that having considered a log-normal distribution on $r_{\rm max}$ with a spread of 0.1, we are nonetheless accounting for possible variations in the SH concentration of about a factor of a few.

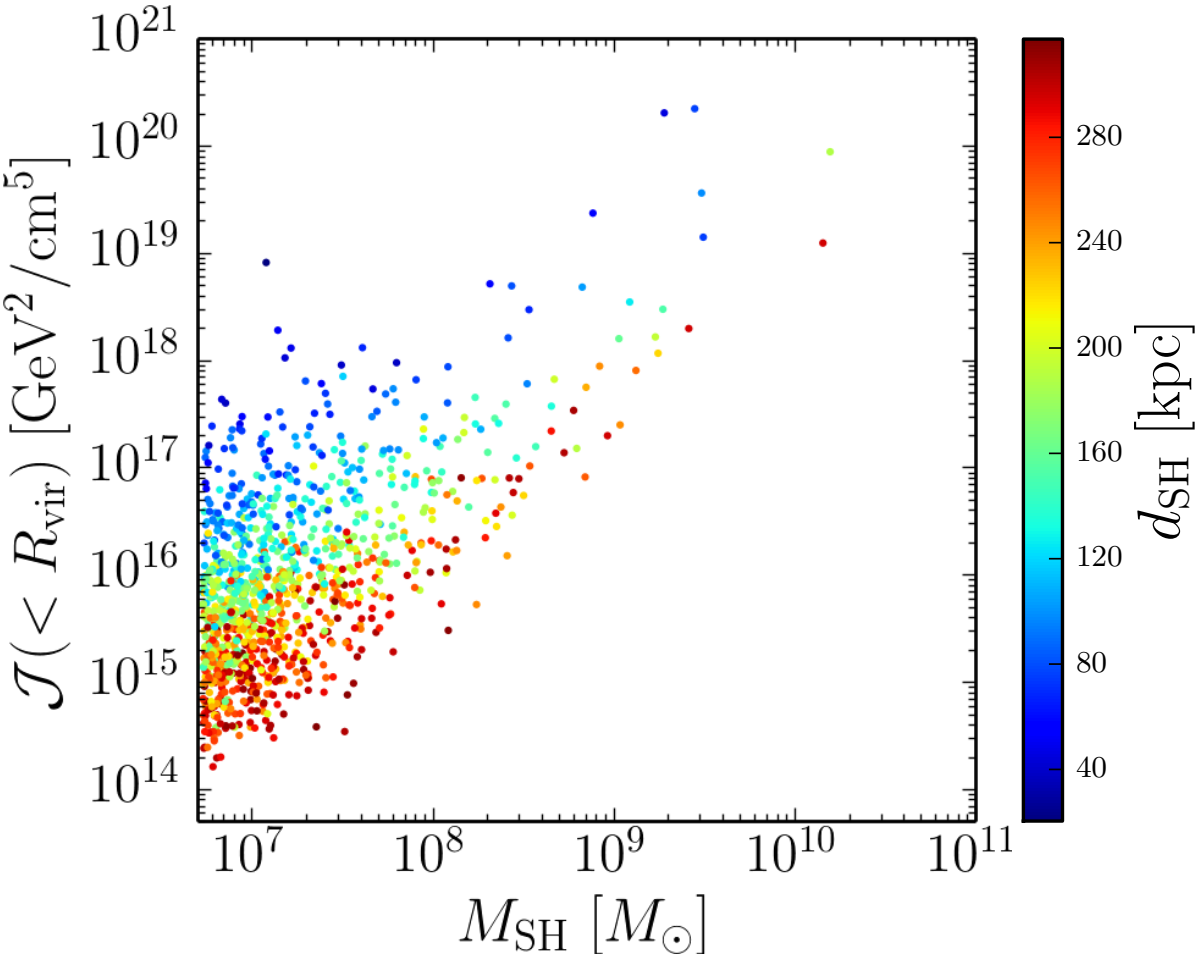

FIG. 3. Scatter plot of $\mathcal{J}$-factor values, $\mathcal{J}$, as a function of the SH mass, $M_{\rm SH}$ in one Hydro realization of our Monte Carlo simulation. The color-bar represents the distance of the SH from Earth, hereafter $d_{\rm SH}$.

Another important ingredient for the determination of the DM annihilation gamma-ray signal is the spectral energy distribution of the signal, the $dN_{\rm DM}/dE$. We will provide in the next section the flux sensitivity to detect a DM SH as a function of the DM channel, mass and Galactic latitude. This result is derived simulating the gamma-ray flux from DM SHs and analyzing the simulations with *Fermi*-LAT Science Tools in order to find significance of their emission. It is thus useful to model the emission from DM annihilation with a spectral shape already included in the Science Tools. Among all the possible functions (see Science Tools[4]) the more flexible is the so called super-exponential cutoff parameterization, given by the following equation [45]:

$$\frac{dN_{\rm DM}}{dE}(E[\rm MeV]) = \rm K \left(\frac{E}{E_0}\right)^{-\Gamma} \exp\left(-\left(\frac{E}{E_{\rm cut}}\right)^{\beta}\right), \tag{8}$$

where $E_0 = 10^3$ MeV is the pivot energy, Γ is the spectral index, $E_{\rm cut}$ is the energy cutoff and β is the curvature index. Depending on the DM mass, $\Gamma = [0.90, 0.10]$ and the spectrum has an exponential cutoff after the peak, which is located at an energy of about $E_{\rm peak} = M_{\rm DM}/20$ for $b\bar{b}$ channel, and $E_{\rm peak} = M_{\rm DM}/3$ for $\tau^+\tau^-$ channel. We perform a fit to the DM annihilation gamma-ray spectra taken from [87] using Eq. (8). This functional form provides a very good fit to DM spectra for all DM masses between 8 and 10^5 GeV. The values of the best-fit parameters are reported in Tab. II for both $b\bar{b}$ and $\tau^+\tau^-$ DM annihilation channels.

[4] `http://fermi.gsfc.nasa.gov/ssc/data/analysis/scitools/source_models.html`

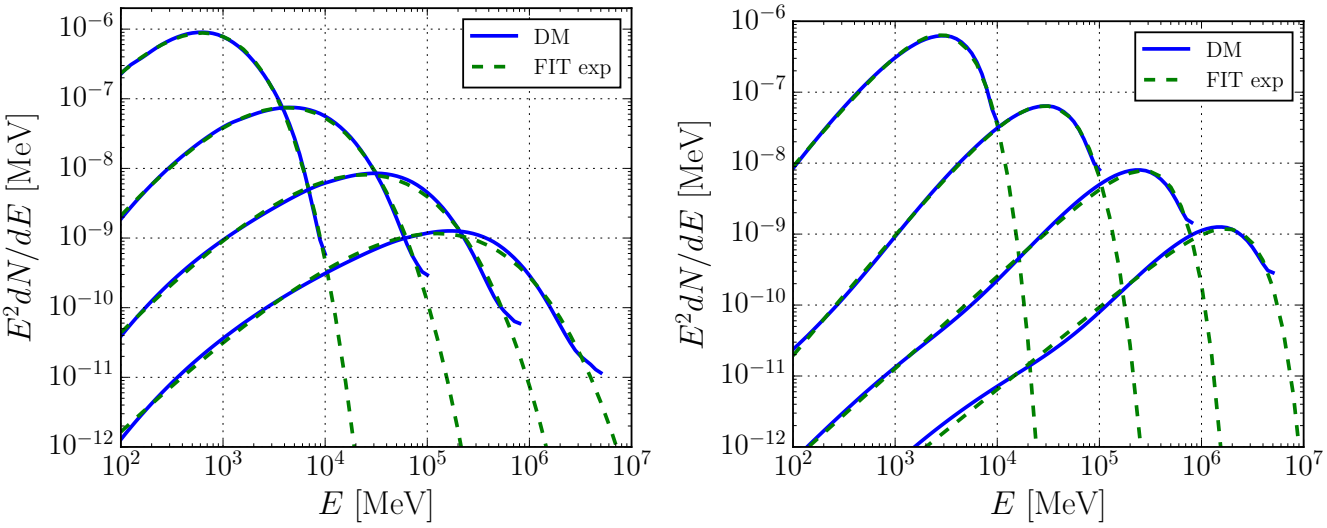

FIG. 4. Fit to DM annihilation gamma-ray spectra from ref. [87] with the super-exponential cutoff function (eq. (8)), for $M_{\rm DM}$ = 10, 100, 800, 5000 GeV (curves from left to right). In the left (right) panel a $b\bar{b}$ ($\tau^+\tau^-$) annihilation channel is assumed. The spectra from ref. [87] are normalized, dividing by the factor ($8 \times \pi \times M^2_{\rm DM}$).

III. *FERMI*-LAT SENSITIVITY TO DARK MATTER SPECTRA

The main aim of this paper is to predict the detectability of Galactic DM SHs, modeled according the latest hydrodynamic simulations, by the *Fermi*-LAT. At this scope we implement, for the first time, the characteristics of both the low-energy 3FGL ($E > 0.1$ GeV) and the high-energy 2FHL ($E > 50$ GeV) *Fermi*-LAT catalogs. One of the main novelties of this paper is the realistic estimation of the flux sensitivity of *Fermi*-LAT to DM SHs detection. The flux sensitivity is defined as the flux at which the Test Statistic (TS)[5] for the SH detection is equal to 25. This is the typical TS value adopted in the *Fermi*-LAT catalogs to claim the detection of sources. Previous works have assumed a fixed threshold to determine the detection of SHs (see e.g. [48, 50]). In this work, we show how the sensitivity flux depends on the DM annihilation channel, DM mass and position of the SH in the sky. The assumption of a fixed sensitivity threshold could turn out to be not accurate enough for the following reasons:

- The spectral representations of sources in *Fermi*-LAT catalog are energy power laws with spectral index Γ ($dN/dE \propto E^{-\Gamma}$), or suitable modifications for correcting curved or exponentially cut-off spectra. The LAT, as shown in [45], has a strong bias for the detection of sources with a given flux as a function of the spectral index. Indeed, the telescope detects more easily lower photon fluxes for sources with harder spectra. This bias could be alleviated considering energy fluxes ($S = \int_{0.1\rm GeV} dN/dE\, E\, dE$) instead of photon fluxes above 100 MeV ($F = \int_{0.1\rm GeV} dN/dE\, dE$), as done in [50], or considering photon fluxes integrated above 1 GeV, as in [48]. However, even when considering photon fluxes for $E > 1$ GeV or energy fluxes, a dependence on the spectrum assumed for the source still remains and, as a consequence, the sensitivity threshold might vary up to a factor of 2 [45]. By assuming a fixed sensitivity threshold, the dependence of the sensitivity itself on the specific source spectrum is ignored, hence leading to possible biases.

- Both the angular resolution and the acceptance of the LAT strongly depend on energy. The angular resolution, for example, is a factor 5 better at 1 GeV than at 100 MeV. This is quite relevant for the detection of DM SHs, since the shape of the DM annihilation gamma-ray energy spectrum changes significantly as a function of the annihilation channel and DM mass. For example, the peak of the spectrum for a DM candidate annihilating into $b\bar{b}$ and with a mass $M_{\rm DM} = 10$ GeV is at a few hundreds MeV, while for $M_{\rm DM} = 100$ GeV the peak appears at few GeV. Indeed, as we will show in the next sections, there is a strong dependence of the sensitivity on the DM particle mass.

- AGN are the most numerous source population detected by the LAT and the estimation of the sensitivity flux from *Fermi*-LAT catalogs is thus mostly related to the gamma-ray spectrum of these objects. However, DM

[5] The TS is defined as TS=2($\log \mathcal{L}(\mu_k) - \log \mathcal{L}(0)$) where $\mathcal{L}(\mu_k)$ is the likelihood for the presence of the source (the spectrum of the source depends on generic parameters μ_k) and $\mathcal{L}(0)$ is the likelihood of the null hypothesis of background only emission (by the interstellar and isotropic emission).

$M_{\rm DM}$	K	Γ	$E_{\rm cut}$	β	K	Γ	$E_{\rm cut}$	β
8	$9.735{\cdot}10^{-11}$	0.096	$7.294{\cdot}10^{1}$	0.594	$8.491{\cdot}10^{-13}$	0.303	$1.676{\cdot}10^{3}$	1.210
10	$4.989{\cdot}10^{-11}$	0.143	$8.624{\cdot}10^{1}$	0.581	$4.833{\cdot}10^{-13}$	0.280	$1.996{\cdot}10^{3}$	1.170
15	$3.435{\cdot}10^{-11}$	0.000	$6.617{\cdot}10^{1}$	0.520	$1.738{\cdot}10^{-13}$	0.223	$2.653{\cdot}10^{3}$	1.093
20	$1.817{\cdot}10^{-11}$	0.000	$6.908{\cdot}10^{1}$	0.498	$8.150{\cdot}10^{-14}$	0.200	$3.313{\cdot}10^{3}$	1.054
30	$7.806{\cdot}10^{-12}$	0.000	$7.021{\cdot}10^{1}$	0.468	$2.691{\cdot}10^{-14}$	0.197	$4.806{\cdot}10^{3}$	1.028
40	$4.109{\cdot}10^{-12}$	0.000	$7.455{\cdot}10^{1}$	0.452	$1.211{\cdot}10^{-14}$	0.210	$6.484{\cdot}10^{3}$	1.026
50	$2.674{\cdot}10^{-12}$	0.000	$7.295{\cdot}10^{1}$	0.437	$6.561{\cdot}10^{-15}$	0.221	$8.187{\cdot}10^{3}$	1.025
60	$1.802{\cdot}10^{-12}$	0.000	$7.487{\cdot}10^{1}$	0.427	$3.960{\cdot}10^{-15}$	0.239	$1.018{\cdot}10^{4}$	1.036
80	$9.890{\cdot}10^{-13}$	0.000	$7.605{\cdot}10^{1}$	0.412	$1.808{\cdot}10^{-15}$	0.273	$1.456{\cdot}10^{4}$	1.063
100	$6.552{\cdot}10^{-13}$	0.000	$7.196{\cdot}10^{1}$	0.398	$9.964{\cdot}10^{-16}$	0.290	$1.880{\cdot}10^{4}$	1.074
150	$2.960{\cdot}10^{-13}$	0.000	$6.834{\cdot}10^{1}$	0.376	$3.557{\cdot}10^{-16}$	0.363	$3.281{\cdot}10^{4}$	1.146
200	$1.669{\cdot}10^{-13}$	0.009	$6.613{\cdot}10^{1}$	0.362	$1.861{\cdot}10^{-16}$	0.437	$5.035{\cdot}10^{4}$	1.226
300	$4.641{\cdot}10^{-14}$	0.142	$1.279{\cdot}10^{2}$	0.368	$8.019{\cdot}10^{-17}$	0.528	$8.753{\cdot}10^{5}$	1.321
400	$2.098{\cdot}10^{-14}$	0.209	$1.842{\cdot}10^{2}$	0.369	$4.603{\cdot}10^{-17}$	0.589	$1.284{\cdot}10^{5}$	1.393
500	$1.134{\cdot}10^{-14}$	0.269	$2.560{\cdot}10^{2}$	0.371	$3.013{\cdot}10^{-17}$	0.627	$1.688{\cdot}10^{5}$	1.431
600	$7.073{\cdot}10^{-15}$	0.305	$3.222{\cdot}10^{2}$	0.372	$2.154{\cdot}10^{-17}$	0.658	$2.113{\cdot}10^{5}$	1.468
800	$3.685{\cdot}10^{-15}$	0.337	$4.000{\cdot}10^{2}$	0.370	$1.273{\cdot}10^{-17}$	0.698	$2.965{\cdot}10^{5}$	1.509
1000	$2.034{\cdot}10^{-15}$	0.397	$5.907{\cdot}10^{2}$	0.372	$8.507{\cdot}10^{-18}$	0.726	$3.823{\cdot}10^{5}$	1.533
1500	$8.566{\cdot}10^{-16}$	0.431	$7.715{\cdot}10^{2}$	0.364	$4.081{\cdot}10^{-18}$	0.766	$5.952{\cdot}10^{5}$	1.555
2000	$4.796{\cdot}10^{-16}$	0.444	$8.698{\cdot}10^{2}$	0.356	$2.407{\cdot}10^{-18}$	0.787	$8.052{\cdot}10^{5}$	1.558
3000	$1.995{\cdot}10^{-16}$	0.491	$1.273{\cdot}10^{3}$	0.353	$1.149{\cdot}10^{-18}$	0.814	$1.228{\cdot}10^{6}$	1.559
4000	$1.155{\cdot}10^{-16}$	0.494	$1.336{\cdot}10^{3}$	0.343	$6.703{\cdot}10^{-19}$	0.827	$1.632{\cdot}10^{6}$	1.535
5000	$7.032{\cdot}10^{-17}$	0.530	$1.822{\cdot}10^{3}$	0.345	$4.473{\cdot}10^{-19}$	0.839	$2.053{\cdot}10^{6}$	1.531
6000	$5.035{\cdot}10^{-17}$	0.527	$1.811{\cdot}10^{3}$	0.337	$3.160{\cdot}10^{-19}$	0.844	$2.444{\cdot}10^{6}$	1.508
8000	$2.944{\cdot}10^{-17}$	0.526	$1.845{\cdot}10^{3}$	0.327	$1.801{\cdot}10^{-19}$	0.849	$3.184{\cdot}10^{6}$	1.461
10000	$1.826{\cdot}10^{-17}$	0.557	$2.488{\cdot}10^{3}$	0.329	$1.185{\cdot}10^{-19}$	0.856	$3.966{\cdot}10^{6}$	1.445
15000	$8.692{\cdot}10^{-18}$	0.554	$2.477{\cdot}10^{3}$	0.314	$5.408{\cdot}10^{-20}$	0.863	$5.759{\cdot}10^{6}$	1.380
20000	$5.204{\cdot}10^{-18}$	0.545	$2.303{\cdot}10^{3}$	0.303	$3.033{\cdot}10^{-20}$	0.864	$7.370{\cdot}10^{6}$	1.315
30000	$2.394{\cdot}10^{-18}$	0.562	$2.745{\cdot}10^{3}$	0.295	$1.359{\cdot}10^{-20}$	0.866	$1.047{\cdot}10^{7}$	1.235
50000	$9.194{\cdot}10^{-19}$	0.574	$3.126{\cdot}10^{3}$	0.284	$5.003{\cdot}10^{-21}$	0.870	$1.581{\cdot}10^{7}$	1.111
100000	$3.213{\cdot}10^{-18}$	0.138	1.230	0.172	$1.910{\cdot}10^{-20}$	0.359	1.000	0.133

TABLE II. Values of the parameters K (in MeV^{-1}), Γ, $E_{\rm cut}$ (in MeV), and β entering the super-exponential cutoff function Eq. (8), from a fit to the gamma-ray spectra from DM annihilation, for $b\bar{b}$ (columns from 2 to 5) and $\tau^+\tau^-$ channels (columns from 6 to 9) at given DM mass $M_{\rm DM}$ (in GeV).

gamma-ray spectra are very different from the spectral energy distribution of AGN. Most of AGN spectra are modeled in the 3FGL with a power law spectra with an average index of about $\Gamma = 2.4$ while, as shown in Sec. II B, the DM spectrum can be well parametrized by a super-exponential cutoff. Therefore, assuming a fixed sensitivity threshold for DM SHs detection based on the sources in the 3FGL and 2FHL catalogs further ignores the dependence on the spectral shape of the signal.

In this section we present the method that we have developed to estimate the flux sensitivity of *Fermi*-LAT to DM SH gamma-ray spectra. We start fully simulating the gamma-ray sky, including the interstellar and isotropic emissions. Then, we simulate DM SHs with different DM masses, both for $b\bar{b}$ and $\tau^+\tau^-$ annihilation channels. We also consider different positions of SHs in the sky, by positioning them at different Galactic latitudes, b. We neglect the longitude dependence of the sensitivity flux because at high latitudes ($|b| > 20^\circ$) the longitudinal variations of the background emissions are negligible compared to the changes induced by variations of the Galactic latitude. In simulating the gamma-ray expected signal we do not include the flux coming from the main Galactic DM halo. For detecting a SH as individual source, this would represent a "background" diffuse emission. As a consequence, it can reduce the sensitivity to SH detection at low latitudes and towards the Galactic center. However, towards the direction of SHs at high latitudes – as the ones studied here – the contribution coming from the main DM halo is usually very

much suppressed with respect to the contribution from the SH, and thus negligible. All-sky gamma-ray maps are created for the same exposure times, energy range and instrument response functions of the two adopted catalogs. Implementing the sensitivity also for the 2FHL catalog (beside the 3FGL one) is motivated by the fact that this is the first *Fermi*-LAT source catalog made with the new Pass 8 event selection. Given the significant improvement of this new dataset, we can provide precise predictions for the detection of DM SHs in an energy range that will be of particular interest for the future Cherenkov Telescope Array observatory [54] (see also ref. [53]).

Operationally, we generate gamma-ray maps of the emission of DM SHs at different latitudes and for different DM channel and masses. We then run the typical detection pipeline in the Binned Likelihood case of the *Fermi*-LAT Science Tools[6], which includes running the *gtselect*, *gtmktime*, *gtbin*, *gtsrcmap* and finally *gtlike* tools. For each DM annihilation channel, DM mass and latitude we derive the flux for which TS=25: this represents the sensitivity flux for that particular DM SH configuration. We note that the uncertainty on the SH flux threshold (also for very bright SHs) depends on the specific run of the *Fermi*-LAT Science Tools and can vary within a factor of about 20%.

In the next two sections we show the results for the sensitivity flux for the 3FGL and 2FHL catalog setups.

A. Sensitivity to dark matter fluxes for the 3FGL catalog setup

In the case of the 3FGL catalog setup we consider 4 years of data (from 2008 August 4, to 2012 July 3) and the energy range $0.1 - 300$ GeV. As done in the 3FGL catalog, in order to reduce the contamination from the Earth limb, events with zenith angles larger than 100° are excised. We simulate the interstellar emission model (IEM) using `gll_iem_v05_rev1.fit`, the isotropic template using `iso_source_v05.txt` and DM SHs at different longitudes and latitudes in the sky. We vary the DM mass between 8 GeV and 10 TeV. We adopt 10 logarithmic bins and a region of interest (ROI) with a radius of 15° around each DM SH, dividing it in spatial bin with size of 0.2×0.2 deg^2. We aim at finding a DM SH flux for different position in the Galaxy, DM mass and annihilation channel, and derive the relation between this flux and the SH TS.

In the left panel of Fig. 5 (Fig. 6) we show the sensitivity flux for $b\bar{b}$ ($\tau^+\tau^-$) for a selection of DM masses, as a function of the Galactic latitude b. In the right panel, we report the same information but fixing two latitude values. For each DM mass, fluxes larger than a specific curve would be detected with TS > 25. That means that a SH made of DM particles of given mass could be resolved by the *Fermi*-LAT (in its 3FGL configuration) if the emitted flux above 0.1 GeV is above that threshold. For both annihilation channels, the flux sensitivity threshold is a mild decreasing function of the latitude. As one moves away from the Galactic plane (i.e. towards high latitudes) the intensity of the IEM decreases and therefore the detection of a fainter halo is easier because of the lower background. Additionally, the dependence of the flux sensitivity threshold on the DM mass is also peculiar: going from 8 GeV to about 300 GeV the sensitivity flux threshold decreases significantly (by a factor of ~ 10), while for DM masses larger than a few hundreds GeV the sensitivity flux decreases only slightly, and settles to values $\sim 10^{-10}$ ph/cm^2/s. On the one hand, for small DM masses the flux sensitivity is larger because the slope of the DM gamma-ray spectrum is softer than for heavier DM masses (cf. Fig. 4) and, as explained above, the LAT detects smaller fluxes for sources with harder spectra at $E > 0.1$ GeV [90]. Moreover, for DM masses above $\mathcal{O}(100)$ GeV the peak of the energy spectrum is at energies where the LAT point spread function (PSF) becomes smaller and the acceptance larger. For example, the peak of the energy spectrum for annihilation into $b\bar{b}$ and DM mass of 10 GeV is at ~ 400 MeV where the PSF is 2° and the acceptance is about 2.25 m^{2}sr. On the other hand, for a candidate with a DM mass of 300 GeV, the gamma-ray energy spectrum peaks at ~ 10 GeV, where the PSF is 0.2° and the acceptance is 2.50 m^{2}sr. The smaller size of the PSF and the larger acceptance explain the order of magnitude of difference in the sensitivity flux threshold between these two cases. Finally, for DM masses larger than 300 GeV the flux sensitivity decreases only mildly, because the PSF and the acceptance at the position of the gamma-ray energy spectrum peak are worse. In this case, only the shape of the energy spectrum matters for the detection and all the considered mass candidates have similar spectral energy distributions.

B. Sensitivity to dark matter fluxes for the 2FHL catalog setup

In this section we report the results for the flux sensitivity for the 2FHL catalog setup. We have considered 80 months of data (from August 2008 to April 2015) and the energy range $50 - 2000$ GeV divided into 5 logarithmic energy bins. The Pass 8 SOURCE class of data has been used with an ROI centered around each DM SH with a radius

[6] `http://fermi.gsfc.nasa.gov/ssc/data/analysis/scitools/binned_likelihood_tutorial.html`

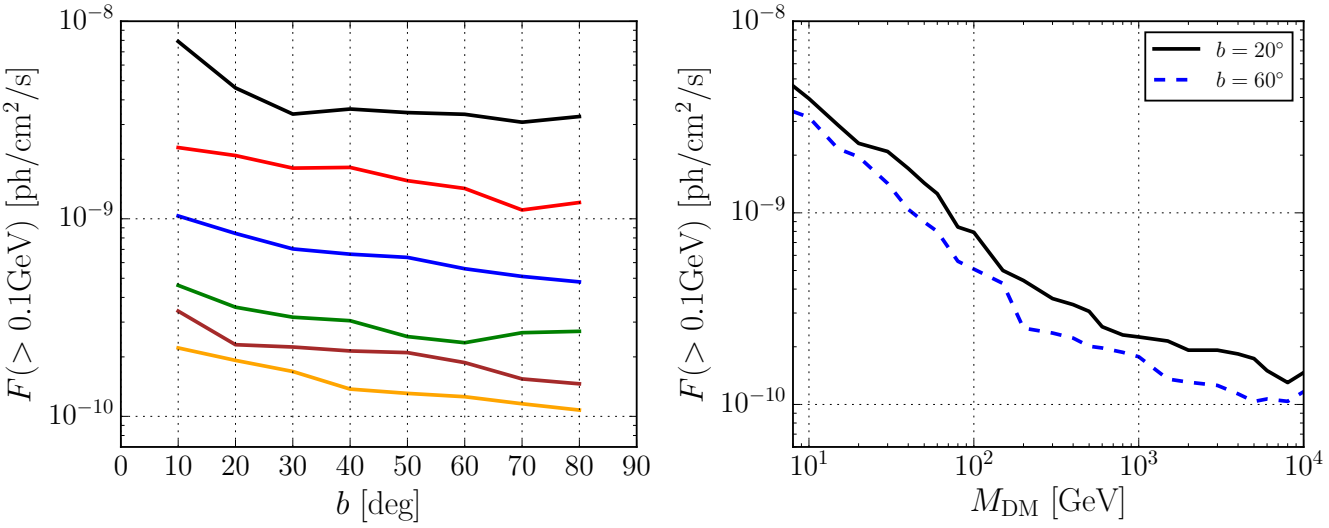

FIG. 5. Flux sensitivity threshold of *Fermi*-LAT 3FGL to DM annihilation spectra for $b\bar{b}$ annihilation channel. *Left panel*: Flux sensitivity threshold as a function of position (latitude) of the SH for, from top to bottom, $M_{\mathrm{DM}} = 8$ (black), 30 (red), 80 (blue), 300 (green), 600 (brown), 1200 (orange) GeV. *Right panel*: Flux sensitivity threshold as a function of DM mass for $b = 20°$ and $60°$ of the SH.

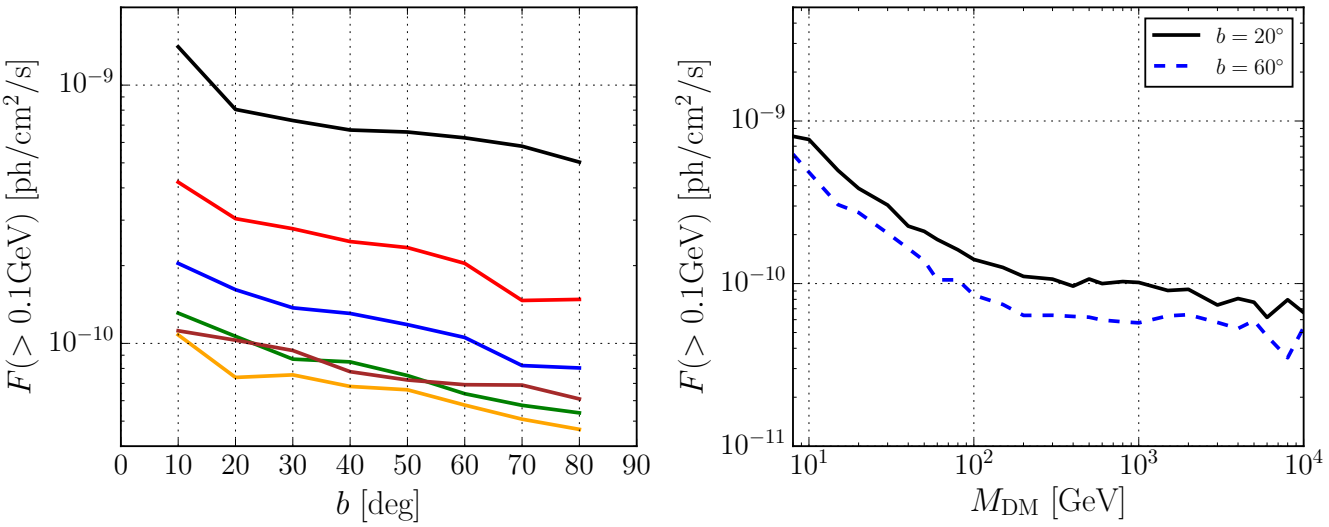

FIG. 6. Same as in Fig. 5 but for $\tau^+\tau^-$ annihilation channel.

of 10° and a spatial binning 0.1×0.1 deg^2. We vary the DM mass between 100 GeV and 100 TeV, since DM masses smaller than 100 GeV have the most of the gamma-ray spectrum below 50 GeV. We use the `gll_iem_v06.fits` and `iso_P8R2_SOURCE_V6_v06.txt` templates. In Fig. 7 (for $b\bar{b}$) and 8 (for $\tau^+\tau^-$) we report the flux sensitivity threshold as a function of latitude for a selection of DM masses (left panels), and as a function of M_{DM} for fixed $b = 60°$ and 20° (right panels). As for the 3FGL, for a fixed mass, the latitude dependence of the sensitivity thresholds mildly improves with increasing latitude because of the reduced contamination from the Galactic emission. The difference between the 2FHL and 3FGL in the slope of the latitude dependence, instead, is due to the interplay between the shape of the DM spectrum and the energy dependence of the background, given the different energy thresholds of the two catalogs. The remaining differences are mild, and we do expect them to be even milder if an average over multiple simulation runs of the sensitivity were performed. However, in the case of the 2FHL, the sensitivity profile shows an opposite trend with respect to the 3FGL case, since it increases with DM mass, reaching a plateau for $M_{\mathrm{DM}} \sim 1$ TeV , regardless of the mass. The flux sensitivity does not change for DM masses $M_{\mathrm{DM}} > 1$ TeV. A DM SH made of TeV mass particles has the same chance to be detected by the *Fermi*-LAT as a $\mathcal{O}(10)$ TeV DM mass SH. The sensitivity flux threshold grows from 100 GeV to 1 TeV because the energy threshold for the 2FHL is 50 GeV. In this energy range and for the considered DM masses, the gamma-ray spectrum has a very soft shape with peak at $E < 50$ GeV.

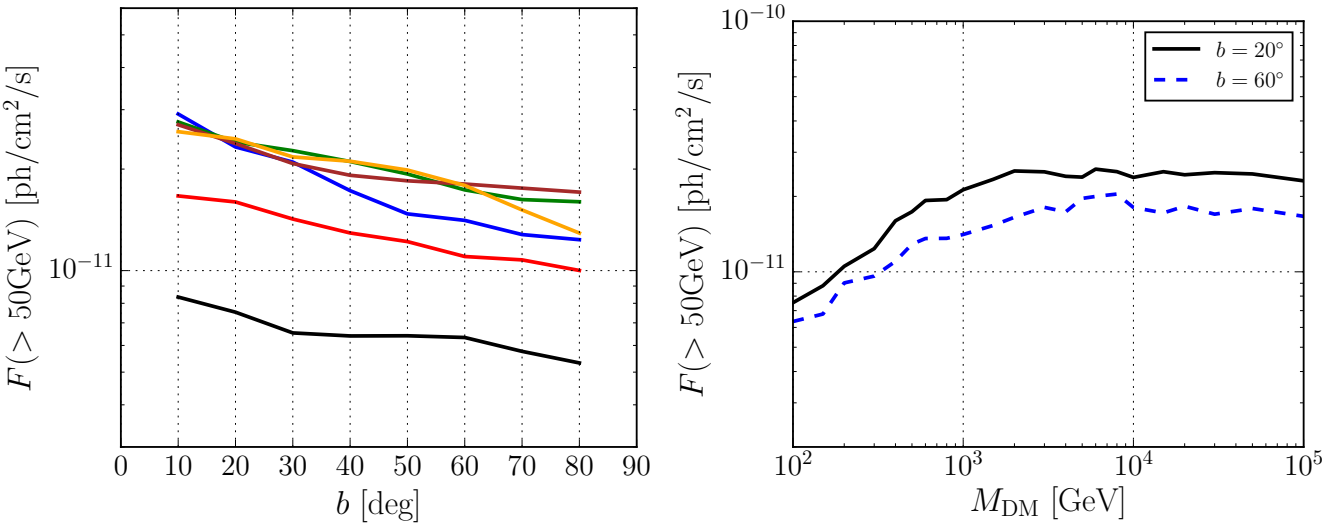

FIG. 7. Flux sensitivity threshold of *Fermi*-LAT 2FHL to DM annihilation spectra for $b\bar{b}$ annihilation channel. *Left panel*: Flux sensitivity threshold as a function of position (latitude) of the SH for, from bottom to top, $M_{\rm DM} = 100$ (black), 400 (red), 1000 (blue), 4000 (green), 8000 (brown), 20000 GeV (orange). *Right panel*: Flux sensitivity threshold as a function of DM mass for $b = 20°$ and $60°$ of the SH.

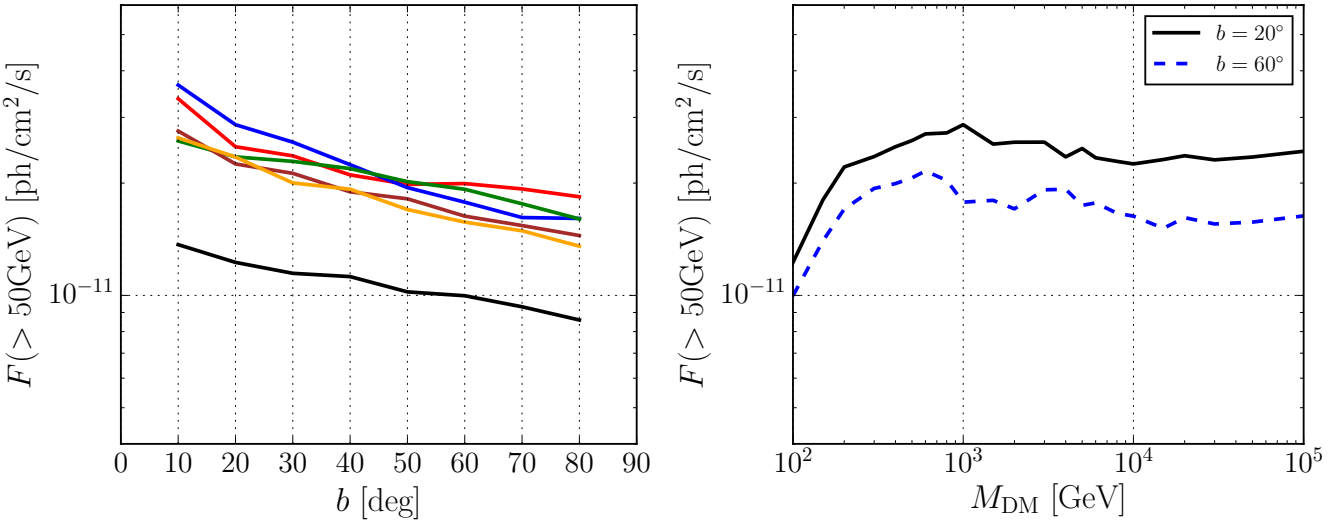

FIG. 8. Same as in Fig. 7 but for $\tau^+\tau^-$ annihilation channel.

Then, for $M_{\rm DM} > 1$ TeV the peak falls inside the 2FHL energy range, the sensitivity flattens and reaches a plateau. For $M_{\rm DM} > 1$ TeV the sensitivity threshold remains constant because the shape of the energy spectrum for these mass candidates is quite similar.

IV. DETECTABILITY OF DARK MATTER SUB-HALOS

In this section we report our results for the detectability of DM SHs. [7] We give our predictions in terms of i) the number of detectable SHs in the 3FGL and 2FHL catalogs setups, ii) bounds on the DM annihilation cross section and iii) the source count distribution of DM SHs, compared to the one of blazars.

[7] We note that we consider here the point-like source detection threshold, i.e. we do not include spatial extension in the analysis of the threshold flux. However, the inclusion of spatial extension would modify our findings only for SHs that can be detected as extended by the LAT. SHs with a size smaller than the LAT angular resolution cannot be resolved as extended, thus the sensitivity and the analysis would not change. As we will present in Sec. V, we expect that only a negligible number of SHs is detectable as extended, when considering cross sections that are not already ruled out by the *Fermi*-LAT analysis of dwarf galaxies.

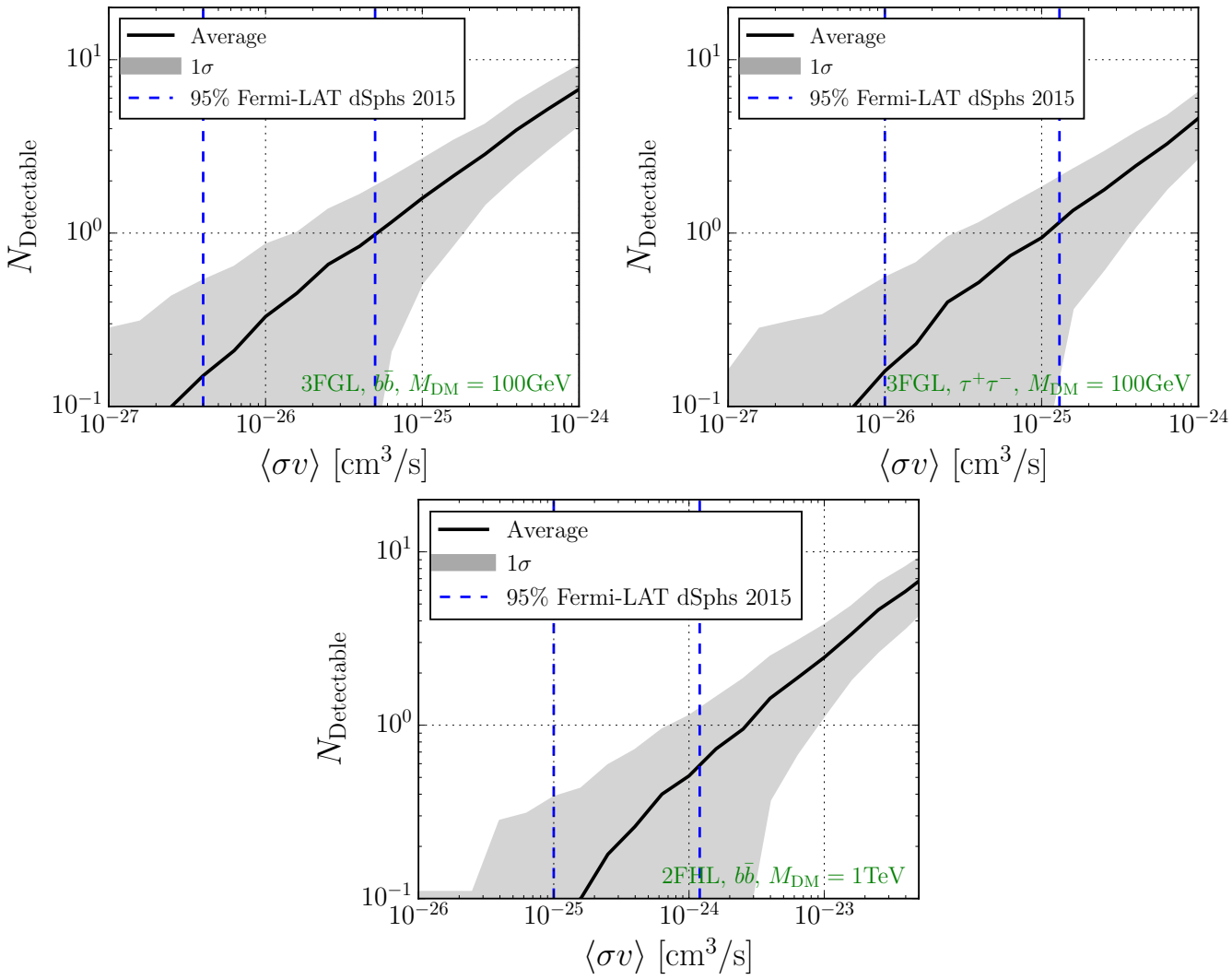

FIG. 9. Number of detectable SHs as a function of the annihilation cross section, $\langle\sigma v\rangle$, for a fixed DM mass value. The black solid line represents the average over 100 Monte Carlo realizations of the SH population, while the grey band is the corresponding 1σ uncertainty. The vertical dashed blue lines are the 95% confidence level cross section upper limits from the *Fermi*-LAT dwarfs analysis [5]. *Top left panel*: $M_{\rm DM}$=100 GeV, 3FGL sensitivity, DM DM $\to b\bar{b}$. *Top right panel*: $M_{\rm DM}$=100 GeV, 3FGL sensitivity, DM DM $\to \tau^+\tau^-$. *Bottom panel*: $M_{\rm DM}$=1 TeV, 2FHL sensitivity, DM DM $\to b\bar{b}$.

A. Number of detectable sub-halos and limits on dark matter annihilation cross section

The SHs that are detectable by the LAT are those with a flux above the *Fermi*-LAT sensitivity flux threshold (for a specific catalog setup) and which could potentially be among the *unassociated* sources in the 3FGL and 2FHL catalogs. The reference *Fermi*-LAT sensitivity fluxes have been discussed in the previous section. While the number of detectable SHs relates to the brightest end of the SH luminosity function, the faintest SHs remain below threshold and thus only contribute to the total SH source count distribution.

In order to derive the number of detectable SHs, for all the SHs in our Monte Carlo realizations (see Sec. II A) we compute the gamma-ray flux above a given energy according to Eq. (6) and assuming an Einasto DM density profile in the SHs. We then compare the predicted flux with the sensitivity flux threshold, depending on the latitude of the individual SH, both for the 3FGL and 2FHL setups, as derived in Sec. III. A SH is defined as detectable if the predicted gamma-ray flux is larger than the sensitivity flux threshold at the SH position.

In Fig. 9, we show the dependence of the number of detectable SHs on the annihilation cross section for different choices of the DM mass, DM annihilation channel and catalog sensitivity. The number of detectable SHs increases with the $\langle\sigma v\rangle$ almost linearly. If we consider the 95% confidence level upper limits on $\langle\sigma v\rangle$ from the *Fermi*-LAT analysis of dwarf galaxies [5], about one SH could be present in the *Fermi*-LAT catalogs.

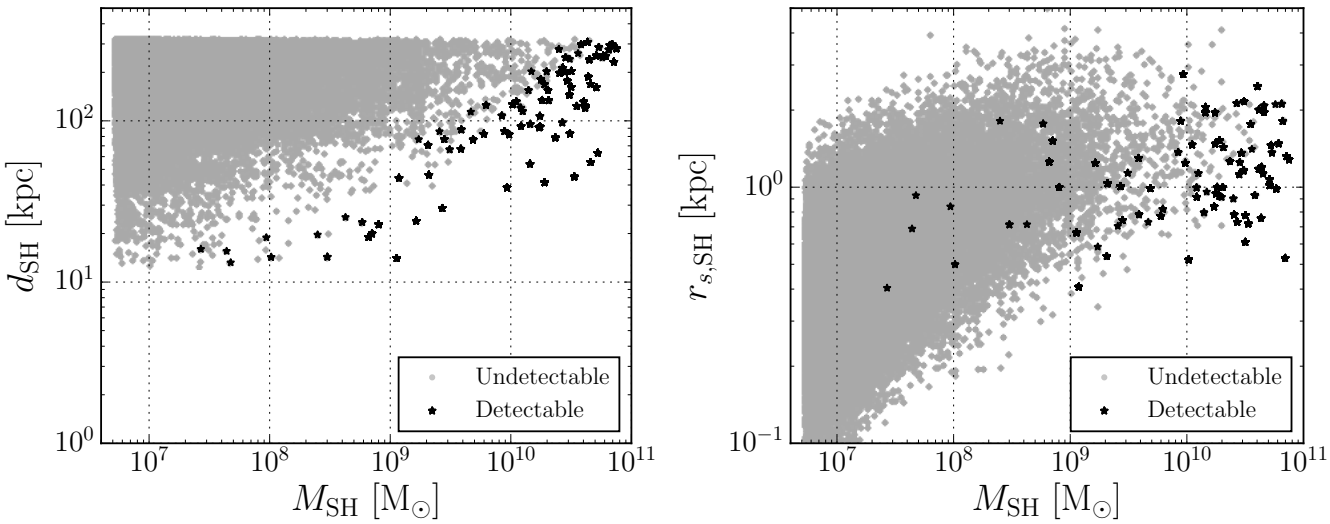

FIG. 10. *Left panel*: SH distance from the observer, $d_{\rm SH}$, as a function of the SH mass, $M_{\rm SH}$, for the detectable SHs (black stars) and the SHs below threshold (grey points). *Right panel*: Scale radius r_s as a function of $M_{\rm SH}$ for the detectable SHs (black stars) and the SHs below threshold (grey points). We adopt the 3FGL sensitivity and DM annihilation into $b\bar{b}$. The results are shown for all 100 Monte Carlo realizations of the SH population. We fix the DM mass to 100 GeV and the annihilation cross section to 3×10^{-26} cm^3/s.

In particular, we checked that, fixing the annihilation cross section to the one constrained by the dwarfs analysis [5] and assuming the 3FGL catalog sensitivity, the number of detectable SHs is only mildly dependent on the DM mass if we assume a $b\bar{b}$ annihilation channel, while it decreases more rapidly as a function of the DM mass for DM DM $\to \tau^+\tau^-$. In the case of the 2FHL, instead, the number of detectable SHs slightly increases with DM mass. However, in all cases we deal with very small numbers of detectable SHs, i.e $\lesssim \mathcal{O}(1)$. The number of detectable SHs that might already be among the unassociated sources of the 3FGL catalog turns out to be 0.9 ± 0.8 for $M_{\rm DM} = 8$ GeV. For the 2FHL, $N_{\rm Detectable}$ is even smaller: 0.0 ± 0.2 for $M_{\rm DM} = 10$ TeV. These are very small numbers compared to the amount of unassociated sources in the 3FGL (1062) and 2FHL (48) catalogs, and are compatible with the fact that no emission from the direction of known dwarf galaxies has been observed yet.

Such small numbers of detectable SHs are lower than what found in the literature, mostly because here we fully model the sensitivity of the *Fermi*-LAT to DM SHs, as explained in Sec. III. We checked that using a fixed energy flux detection threshold – as given by the energy flux integrated above 1 GeV[8] and equal to the minimum flux of sources (in the 3FGL), $4.0 \cdot 10^{-13}$ erg/cm^2/s – we get twice more detectable SHs. On the other hand, using the energy flux that gives the peak of the energy flux distribution, namely $1.35 \cdot 10^{-12}$ erg/cm^2/s, leads to 20% less detectable SHs for $M_{\rm DM} = 100$ GeV with respect to the former optimistic threshold.

In Fig. 10 we display the distance to the observer $d_{\rm SH}$ vs the mass $M_{\rm SH}$ for all SHs in our 100 Monte Carlo realizations, and highlight the ones with a flux larger than the *Fermi*-LAT 3FGL sensitivity flux. We fix the DM mass to 100 GeV and the annihilation cross section to 3×10^{-26} cm^3/s. We obtain few detectable SHs (depicted with black stars), with distances $d_{\rm SH} \in [10, 300]$ kpc and $M_{\rm SH} > 2 \cdot 10^7 M_\odot$. Contrary to what assumed in previous analyses (see e.g. [48]) we find that the detectable dark and luminous SHs may be more massive than $\sim 10^7$ $M_\odot$. We wish to stress that even if the minimum mass for SHs to host star formation is about $10^{7.5}$ $M_\odot$, dark SHs (i.e. without stars) are realized in the simulation up to masses $\sim 10^9$ $M_\odot$, and hence coexist together with luminous SHs in the mass range $10^{7.5} h^{-1} - 10^9 h^{-1} M_\odot$ [57]. Larger mass SHs are instead much more likely to have a stellar counterpart and therefore to be detected in the optical wavelength as dwarf galaxies. We also show in Fig. 10 the value of the scale radius r_s of each SH vs the SH mass. The smallest r_s values correspond to undetectable SHs, independently of $M_{\rm SH}$. Detectable SHs can have r_s ranging from 0.4 kpc to 3 kpc, regardless the value of the SH mass. We note that, in general, smaller values of r_s correspond to larger concentration parameters, and hence to larger DM signals emitted at fixed mass. However, also the distance plays a role in the determination of the detectability and the results in Fig. 10 are indeed based on this interplay. Still, a relic of the fact that a larger concentration should lead to more easily detectable objects can been seen in Fig. 10 (right): the detectable SHs populate the lower part of the r_s distribution – so smaller r_s are favoured in a regime in which the SH might be detectable.

[8] We use this quantity in order to reduce the bias between the source flux and the photon index, see [90].

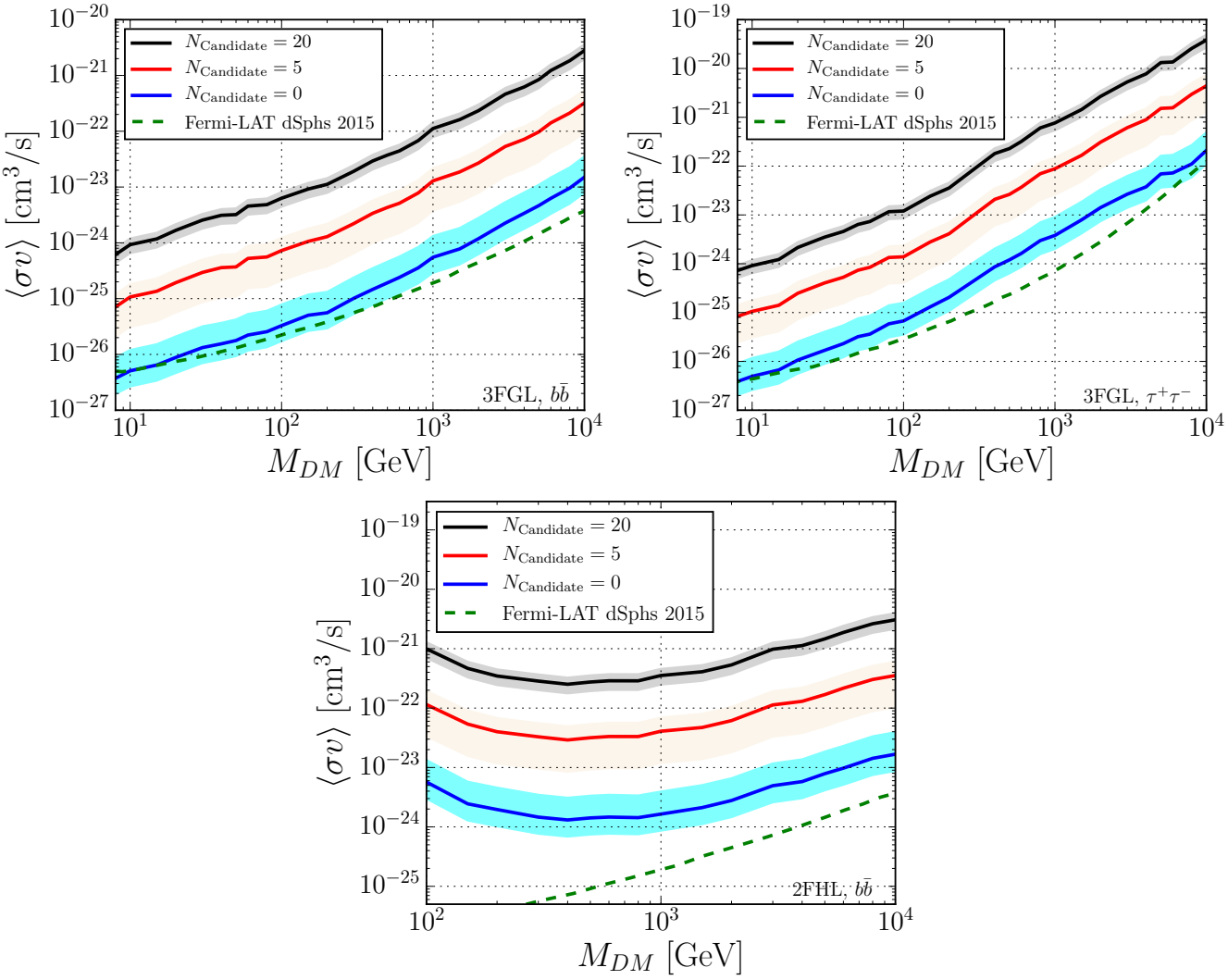

FIG. 11. Upper limits on $\langle\sigma v\rangle$ derived assuming 20 (grey), 5 (red) and 0 (cyan) SHs candidates in *Fermi*-LAT catalogs, together with the bounds from the dwarf galaxies *Fermi*-LAT analysis [5]. *Top left (right) panel*: Annihilation into $b\bar{b}$ ($\tau^+\tau^-$) and 3FGL catalog setup. *Bottom panel*: Annihilation into $b\bar{b}$ and 2FHL catalog setup.

The small (or even null) number of detectable DM SH candidates among the *Fermi*-LAT unassociated sources allows us to set upper limits on the DM annihilation cross section $\langle\sigma v\rangle$. For each DM mass, we define as upper limit the value of $\langle\sigma v\rangle$ for which the number of detectable SH is smaller than a given number $N_{\rm Candidate}$ of DM SH candidates. Should $N_{\rm Candidate}$ be zero, the most stringent constraints on $\langle\sigma v\rangle$ would be inferred. However, the number of unassociated sources in the two catalogs is not zero, and we do expect some DM SHs among them. Indeed, the case in which $N_{\rm Candidate} = N_{\rm Unassociated}$ would give the most conservative upper limits, not accounting for the fact that many unassociated sources are very likely going to be identified as standard astrophysical objects.

In the following, we will show upper limits on $\langle\sigma v\rangle$ assuming $N_{\rm Candidate} = 0$, 5 and 20. We consider the number $N_{\rm Candidate}$ of brightest SHs (in terms of $\mathcal{J}$-factor) for all the 100 Monte Carlo realizations, and we define the upper limit on $\langle\sigma v\rangle$ as the maximum value of $\langle\sigma v\rangle$ for which the SHs fluxes are equal to the sensitivity flux thresholds – for a given catalog – at the corresponding SHs position. We depict in Fig. 11 the upper bounds on the $\langle\sigma v\rangle$, assuming the possible detection of 0 (cyan), 5 (red) and 20 (grey) SHs, for the 3FGL catalog setup (upper panels) and DM annihilation channel into $b\bar{b}$ (left panel) or $\tau^+\tau^-$ (right panel), and for the 2FHL catalog setup for $b\bar{b}$ annihilation channel (bottom panel). The bounds for the detection of $N_{\rm Candidate} = 5$ and 20 result weaker than those derived with the Pass 8 analysis of dwarf galaxies [5]. On the contrary, the limits derived assuming $N_{\rm Candidate} = 0$ are very tight and competitive with limits from dwarfs galaxies. The reason is that the brightest SH in all realizations has a very high flux. For example, the gamma-ray flux of the brightest SH with DM mass of 100 GeV and with thermal cross section is on average 1.6×10^{-9} ph/cm^2/s, thus above the sensitivity threshold at b=30° ($\sim 7 \times 10^{-10}$ ph/cm^2/s,

cf. Fig. 5).

The dependence of the cross section upper limits on the DM mass can be understood as follows: The annihilation cross section is derived from Eq. (6) as $\langle\sigma v\rangle \approx (\Phi 4\pi M_{\rm DM}^2)/(\mathcal{J}\mathcal{I})$, and, taking into account only the quantities dependent on the DM mass, $\langle\sigma v\rangle \propto (\Phi M_{\rm DM}^2)/(\mathcal{I})$. The integrated gamma-ray energy spectrum from DM annihilation for $b\bar{b}$ channel is $\mathcal{I} \propto M_{\rm DM}^{0.4}$. On the other hand, the sensitivity flux goes as $\Phi \propto M_{\rm DM}^{-0.8}$ for $M_{\rm DM} < 100$ GeV and $\Phi \propto M_{\rm DM}^{-0.4}$ for $M_{\rm DM} > 100$ GeV (see Fig. 5). Therefore, $\langle\sigma v\rangle \propto M_{\rm DM}^{0.8}$ for $M_{\rm DM} < 100$ GeV and $\langle\sigma v\rangle \propto M_{\rm DM}^{1.2}$ for $M_{\rm DM} > 100$ GeV, as shown in Fig. 11.

In full analogy, it is possible to explain the trend of the upper limits in the case of the 2FHL. In this case, for $M_{\rm DM} \in [100, 500]$ GeV, $\mathcal{I} \propto M_{\rm DM}^{3.0}$ and $\Phi \propto M_{\rm DM}^{0.6}$ so that the annihilation cross section decreases as $\langle\sigma v\rangle \propto M^{-0.4}$. On the other hand, for $M_{\rm DM} > 500$ GeV the flux sensitivity flattens (see Fig. 8) and $\mathcal{I} \propto M_{\rm DM}^{1.0}$, so that roughly $\langle\sigma v\rangle \propto M^{1.0}$ as observed in Fig. 11 (bottom panel).

With a larger number of DM SHs candidates, the bounds reported in Fig. 11 get looser and increase less steeply. This fact has important consequences: First of all, in the 3FGL catalog there are about 1000 unassociated sources and decreasing this number – even by a factor of 10 – would not have a large impact on the upper limits inferred on $\langle\sigma v\rangle$. On the other hand, in the 2FHL catalog there are about 50 unassociated sources: reducing the number of unassociated sources in this catalog by a factor of two would improve the bounds on $\langle\sigma v\rangle$ by a factor of almost 10.

Future gamma-ray experiments, such as CTA [54] at TeV energies and new concept Compton-Pair Production Telescopes like Compair [91] and e-ASTROGAM [92] at the MeV scale, will improve on the sensitivity to detect point sources and DM SHs. As mentioned in Sec. II A, DM SHs are classified into dwarf galaxies (i.e. luminous SHs) or dark SHs according to the presence or absence of a stellar component. The lower (non-zero) stellar mass of the Hydro selected SHs is $1.4 \times 10^4 M_\odot$. We here estimate the probability to detect dwarf galaxies as DM SHs with a future gamma-ray instrument with a factor of 5 better sensitivity than the LAT above 100 MeV. This improvement could be achieved by e-ASTROGAM or Compair at MeV energies. We consider DM annihilation into $b\bar{b}$ for DM mass of 100 GeV and thermal cross section. In the Hydro simulation, the fraction of luminous SHs in the mass bins $M_{\rm SH} = [10^{6.7} - 10^7, 10^7 - 10^8, 10^8 - 10^9, 10^9 - 10^{10}, 10^{10} - 10^{11}]$ is $N_{\rm SH}(M_* \geq 1.4 \times 10^4 M_\odot)/N_{\rm SH} = [0.000, 0.024, 0.409, 0.857, 1.000]$. Running our analysis for the SHs detectability with an improved flux sensitivity, we find that the average number of detectable SHs in each bin of mass is [0.0, 0.24, 0.34, 0.57, 0.91]. Combining these two results together, we obtain that 2.1 SHs would be detectable on average and 1.5 out of these would be dwarf galaxies. Therefore, given the input of the adopted simulation, a future gamma-ray experiment a factor of 5 more sensibile than the LAT has the power to detect a few SHs, with a probability of 75% to detect a dwarf galaxy.

B. The Log N – Log F relationship for dark matter sub-halos

An important characterization of astrophysical source populations is given by the so-called Log N – Log F, or the source count distribution N as a function of the integrated flux F, which can provide information also about the faintest end of the flux distribution for a specific source population.

For all the simulated SHs in the 100 Monte Carlo realizations of a Galactic SH population, we compute the photon flux F as given by Eq. (6). We derive dN/dF choosing a binning of the photon flux and considering for each i-th bin $\frac{dN}{dF}(F_i) = N_i/\Delta_i$, where F_i is the center of the flux bin with a width Δ_i and N_i is the number of SHs with a given flux in that bin. For each flux bin we compute the mean and the standard deviation of N_i over all Monte Carlo realizations, and we estimate the average and the 1σ dispersion for the dN/dF. Finally, we compare this result with the same observable derived for AGN in the 1FGL [90] and 2FHL [93] catalogs.

In Fig. 12 we show the Log N – Log F of all simulated DM SHs, with integrated flux above 0.1 GeV and 50 GeV respectively for the 3FGL (left panel) and 2FHL (right panel) catalog setups. For comparison, we overlay the expected source count distribution from blazars in the 1FGL [90] and the recent estimate for high-energy blazars from the 2FHL [93]. We consider annihilation into $b\bar{b}$ and DM mass of 100 GeV for the 3FGL and the 2FHL. The cross section is fixed to $\langle\sigma v\rangle = 10^{-25}$ cm^3/s. The Log N – Log F of DM SHs shows a sharp cutoff at high fluxes, that corresponds to few very bright SHs – in the case of the chosen annihilation cross section this is at about 5×10^{-7} (5×10^{-9}) ph/cm^2/s for integrated fluxes above 0.1 (50) GeV. The numerous faint and undetectable SHs populate the Log N – Log F at low fluxes. Regardless of the choice of the integration energy threshold, the SHs source count is strongly subdominant with respect to the observed flux distribution of AGN in both the 3FGL and 2FHL catalogs. This effect becomes stronger when considering lower values of $\langle\sigma v\rangle$, which are consistent with current limits from dwarf galaxies.

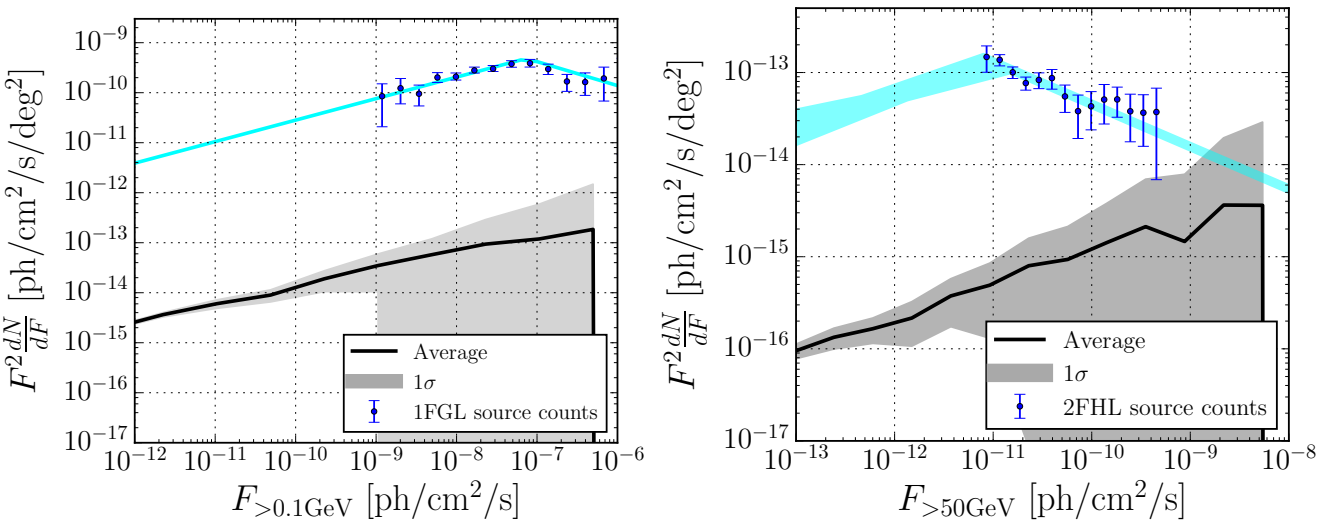

FIG. 12. Source count distribution, or Log N – Log F, of all SHs in the mock Galactic SH population for DM annihilation into $b\bar{b}$. *Left panel*: 3FGL catalog setup, $M_{\rm DM}$=100 GeV and $\langle\sigma v\rangle = 10^{-25}$ cm^3/s. The blue solid line represents the best-fit to the Log N – Log F of the blazars population in the 1FGL [90]. The black solid line is the average over 100 Monte Carlo realizations of the SH populations, while the grey band is the corresponding 1σ uncertainty. *Right panel*: Same as in the left panel but with the 2FHL catalog setup and source count distribution of blazars as derived in ref. [93].

C. On the relevance of the smaller scales: $M_{\rm SH} > 10^5\ M_\odot$

As already mentioned in Sec. II, the hydrodynamic simulation studied in this work has a mass resolution of $5.4 \times 10^6\ M_\odot$. Although we are mostly interested in analyzing the differences between the Hydro and DMO runs, usually expected to be important for quite massive SHs, we anyhow investigate the effect of lower-mass SHs. We proceed arguing for the Hydro case only.

Adopting the prescriptions outlined in Sec. II, we simulate on average 38000 SHs from $10^5\ M_\odot$ (which is the mass resolution of AQ08) up to $5.4 \times 10^6\ M_\odot$, and derive r_s from $r_{\rm max}$ by extrapolating to low masses its polynomial dependence on $M_{\rm SH}$ as described in Sec. II A. The results of this new Monte Carlo realization are presented in Fig. 13, for DM annihilating into $b\bar{b}$ and mass $m_{\rm DM} = 100$ GeV, and for 3FGL catalog setup. We show the average Log N – Log F of the SHs with masses $\geq 5.4 \times 10^6\ M_\odot$ (as resolved by the original simulation) as red dashed line and the average Log N – Log F of the SHs with masses $10^5 \leq M_{\rm SH} \leq 5.4 \times 10^6\ M_\odot$ as a green dashed line. The black line shows the total source count distribution from the sum of the two populations of SHs. For the sake of comparison, we further show as blue line the expected source count distribution from blazars in the 1FGL [90]. Adding lower-mass SHs increases the number of sources per unit flux at very small fluxes. This fact has no impact on the number of detectable SHs nor on the constraints on the annihilation cross section. This result is consistent with Fig. 10, where SHs with $M_{\rm SH} < 10^7\ M_\odot$ (thus well above the mass resolution of the simulation) are not detectable as point sources. Nonetheless, those SHs would unavoidably contribute to the diffuse gamma-ray emission [41]. Although very challenging because of the many theoretical uncertainties, and of the unavoidable contribution from unresolved blazars and Misaligned AGN (see e.g. [59, 60]), it is possible to look for those unresolved SHs in the intensity [40] and small scale fluctuations [44] of the gamma-ray sky. While we do not address this search here, it will be certainly an interesting topic to explore in future work.

V. SPATIAL EXTENSION OF DARK MATTER SUB-HALOS

In this section we discuss one of the clearest signatures for the detection of a DM SH as a gamma-ray source: its spatial extension. Indeed, should an unassociated source be detected by the LAT with a non-zero spatial extension at high latitude, it would be a tantalizing hint of a signal from DM SH. Up to now only associated astrophysical objects have been found as extended, and no unassociated object has been detected with a spatial extension. Estimations of the number of extended SHs that could be detected in the 3FGL have been performed in previous works comparing the scale radius r_s with the size of the PSF. Ref. [50], for example, employs the parameter $R_{\rm ang} = \arctan\left(r_s/d_{\rm SH}\right)$ to perform the analysis of the spatial extension. This parameter represents the angular size associated to the scale radius

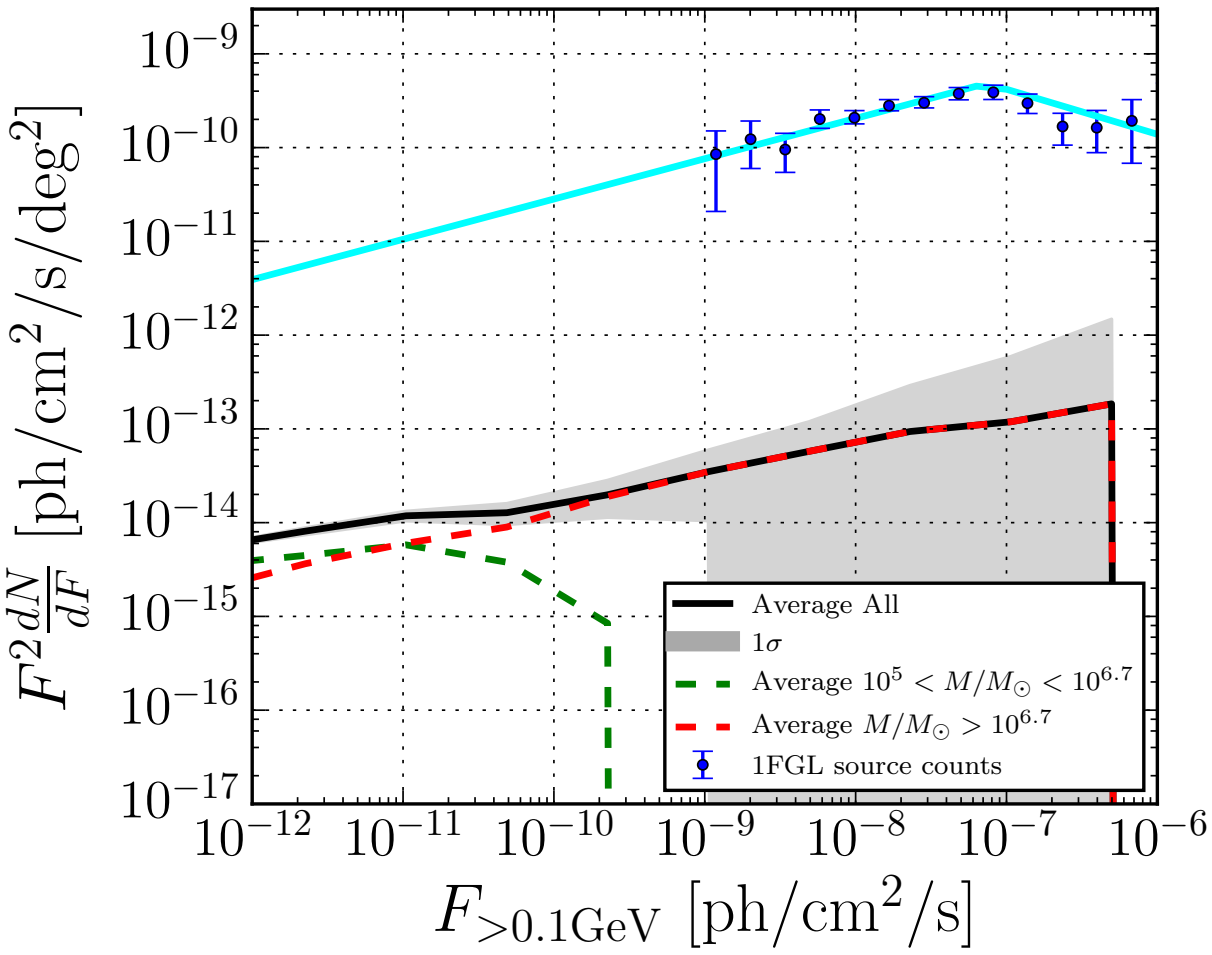

FIG. 13. Same as left panel in Fig. 12, for $M_{\rm SH} \geq 10^5 M_\odot$ (mass resolution of AQ08). We show separately the contribution of $10^5 M_\odot \leq M_{\rm SH} < 10^{6.7} M_\odot$ (green dashed line), and $M_{\rm SH} \geq 10^{6.7} M_\odot$ (mass resolution of Hydro AQ, red dashed line).

of the SH. $R_{\rm ang}$ is then compared to the size of the PSF for `P7REP_SOURCE_V15`, which at 1 GeV is 0.8°. Nevertheless, the definition of $R_{\rm ang}$ is not precisely comparable with the way extended sources are studied in the 3FGL catalog. Indeed the size of 3FGL extended sources is determined as the angle $\Theta_{\rm ext}$ inside which the 68% of the gamma-ray intensity is contained.

We calculate here the gamma-ray flux for different angular distances from the center of each DM SH and we infer the angular distance $d^{68}_{\rm SH}$ inside which the 68% of the gamma-ray flux is contained, analogously to the definition in ref. [51]. However, we choose a different approach to estimate the sensitivity of the LAT to detect extended sources. We use the extension of 3FGL sources and the error on their position to estimate the angular extension sensitivity of the telescope. First of all, we note that the angular extension of the least extended 3FGL sources is between $0.14° - 0.20°$ for W44 and 0.16° for HESS J1303-631 [45]. We can then infer the error on the determination of the position of 3FGL sources (at $|b| > 20°$), using the parameter `Conf_68_Semiminor`, reported in *Fermi*-LAT catalogs (see e.g. [45]) to parametrize the 68% confidence level of the dimension of the source if modeled with an ellipse. This parameter is $\sim 0.10°$ for most sources with TS = 25 and $|b| > 20°$. This value can be used as an estimation of the lower limit on the spatial extension of a source that can be found in the 3FGL.

We follow two approaches: A conservative one, where we take as a reference angle for the SH spatial extension the size of W44 ($\Theta_{\rm ext} = 0.16°$), and a more optimistic choice where we consider the average value of `Conf_68_Semiminor` for sources with TS = 25 in the 3FGL ($\Theta_{\rm ext} = 0.10°$), as done also in ref. [51]. The latter choice is nevertheless not too optimistic, if we consider that with Pass 8 PSF Type 3 (the PSF quality quartile with the best angular resolution[9]) there is an improvement with respect to the 3FGL (Pass 7) of at least a factor of two in angular resolution. If $d^{68}_{\rm SH}$

[9] `https://www.slac.stanford.edu/exp/glast/groups/canda/lat_Performance.htm`

is larger than $\Theta_{\rm ext}$, then the SH is considered extended. We analyze only SHs with a flux larger than the sensitivity flux threshold derived for the 3FGL catalog setup.

Working with all 100 Monte Carlo realizations, a DM mass $M_{\rm DM} = 40$ GeV, annihilation into $b\bar{b}$ and the thermal cross section we have on average, for each realization, 0.5 extended sources when conditioned to $\Theta_{\rm ext} = 0.16^\circ$, while using the optimistic approach ($\Theta_{\rm ext} = 0.10^\circ$) we get 0.8 extended sources per realization. These estimated numbers for extended sources in the 3FGL catalog are smaller than what has been derived in ref. [50], where 4 extended objects were predicted (assuming $M_{\rm DM} = 40$ GeV and thermal annihilation cross section). Indeed, the sensitivity flux threshold used in the analysis performed by [50] is different and, as we have shown in the previous sections, this brings to different predictions in the number of detectable SHs. We are as well using a different approach to define whether a DM SH can be detected as extended source.

The DM SHs that we find to be extended show the following features: $M_{\rm SH} > 2 \cdot 10^7 M_\odot$ and distance < 80 kpc. On average, the smaller is the mass of the extended SH, the smaller is the distance. For example, SHs with $M_{\rm SH} \sim 1 \cdot 10^8 M_\odot$ are at most located on average at 30 kpc of distance, while less massive objects with $M_{\rm SH} \sim 2 \cdot 10^7 M_\odot$ can be as far as 15 kpc.

In Fig. 14 we show the flux profile as a function of the angular separation for two extended SHs: the first (SH 1) has a mass $M_{\rm SH} = 1.9 \cdot 10^9 M_\odot$, $r_s = 1.1$ kpc and $d_{\rm SH}$ =46 kpc, the second (SH 2) has a mass $M_{\rm SH} = 4.7 \cdot 10^9 M_\odot$, $r_s = 1.4$ kpc and $d_{\rm SH} = 80$ kpc. We highlight in the same plot the angular distance $\Theta_{\rm ext}$ for our optimistic and conservative scenarios. The angular profile for DM SHs has a steeply decreasing shape that is much different than a Gaussian profile, as it can be seen from the figure. This intrinsic distribution, once convolved with the LAT PSF, would show the sharp peak smoothed over a larger solid angle, making the angular emission more similar to a Gaussian function. The presence (and shape) of the extension by itself is not sufficient to claim an evidence of DM SH. Would a source be detected as extended, it should be an unassociated source in the 3FGL *and* future *Fermi*-LAT catalogs before being claimed a possible DM SH . An additional remark is that given the improvement in the LAT sensitivity with Pass 8, future catalogs will contain many more sources than the 3FGL catalog. With an increasing number of detected sources, the probability of having two gamma-ray sources detected with a distance of the order of the LAT PSF, and thus looking as a single extended source, is not negligible. This hypothesis therefore should be considered when an extended unassociated *Fermi*-LAT source will be discovered, and even more if the source spectrum will show a good match with a DM-like spectrum.

VI. SUMMARY AND CONCLUSIONS

We have presented a realistic estimation of the detectability of Galactic dark matter sub-halos in the *Fermi*-LAT 3FGL and 2FHL catalogs. Based on one of the most recent hydrodynamic simulations for structure formation, the Hydro-Aquarius simulation [1, 57], we have modeled the spatial and mass distribution of sub-halos in a Milky Way-like Galaxy. We have generated Monte Carlo realizations of the Galactic sub-halo population (with minimum mass $M_{\rm SH} \sim 5 \times 10^6\ M_\odot$) for the hydrodynamic and pure dark matter scenarios. Our first motivation was to investigate the impact of hydrodynamics on the distribution and properties of Galactic dark matter sub-halos, and consequently on the gamma-ray signal expected from those structures. At this scope, we have compared the scale radius typical of each sub-halo, deeply related to the sub-halo mass accretion history and to the concentration parameter. Being a physical parameter of the radial sub-halo density, it is indeed a crucial quantity for the determination of the gamma-ray flux. We modeled r_s directly from the simulation data of $r_{\rm max}$. Although baryons affect the abundance and internal structure of sub-halos (especially the more massive ones), these discrepancies do not substantially alter the predictions on r_s. This conclusion holds as well for the geometrical factor $\mathcal{J}$-factor, which is a direct measure of the intensity of the gamma-ray signal.

In order to estimate the realistic sensitivity for the *Fermi*-LAT to detect dark matter sub-halos, we have introduced some novelties. In particular, we fully account for dependence of the sensitivity flux threshold on the dark matter annihilation channel, the dark matter mass and the sub-halo position in the main halo. We have overcome the simplistic approach of considering a fixed sensitivity flux threshold, showing in particular the strong dependence of the sensitivity flux threshold on the dark matter mass. Moreover, we have presented the prospects of detection of sub-halos among the unassociated sources of two *Fermi*-LAT catalogs: probing different energy ranges, the results for 3FGL and 2FHL result complementary.

We have studied the dark matter annihilation gamma-ray signatures, from Galactic sub-halos in terms of: (1) the number of detectable sub-halos in the two catalogs, (2) the bounds on the dark matter annihilation cross section, (3) the source count distribution and (4) the sub-halos extension. Our results show that the largest number of detectable sub-halos, that might already be among the unassociated sources of the 3FGL catalog, is at most 0.9 ± 0.8 for $M_{\rm DM} = 8$ GeV – with $\langle \sigma v \rangle$ fixed to the upper limit derived from the latest analysis of dwarf spheroidal galaxies. The prediction for the 2FHL catalog is lower: $N_{\rm Detectable} = 0.0 \pm 0.2$ for $M_{\rm DM} = 10$ TeV. These tiny numbers allow to set constraints

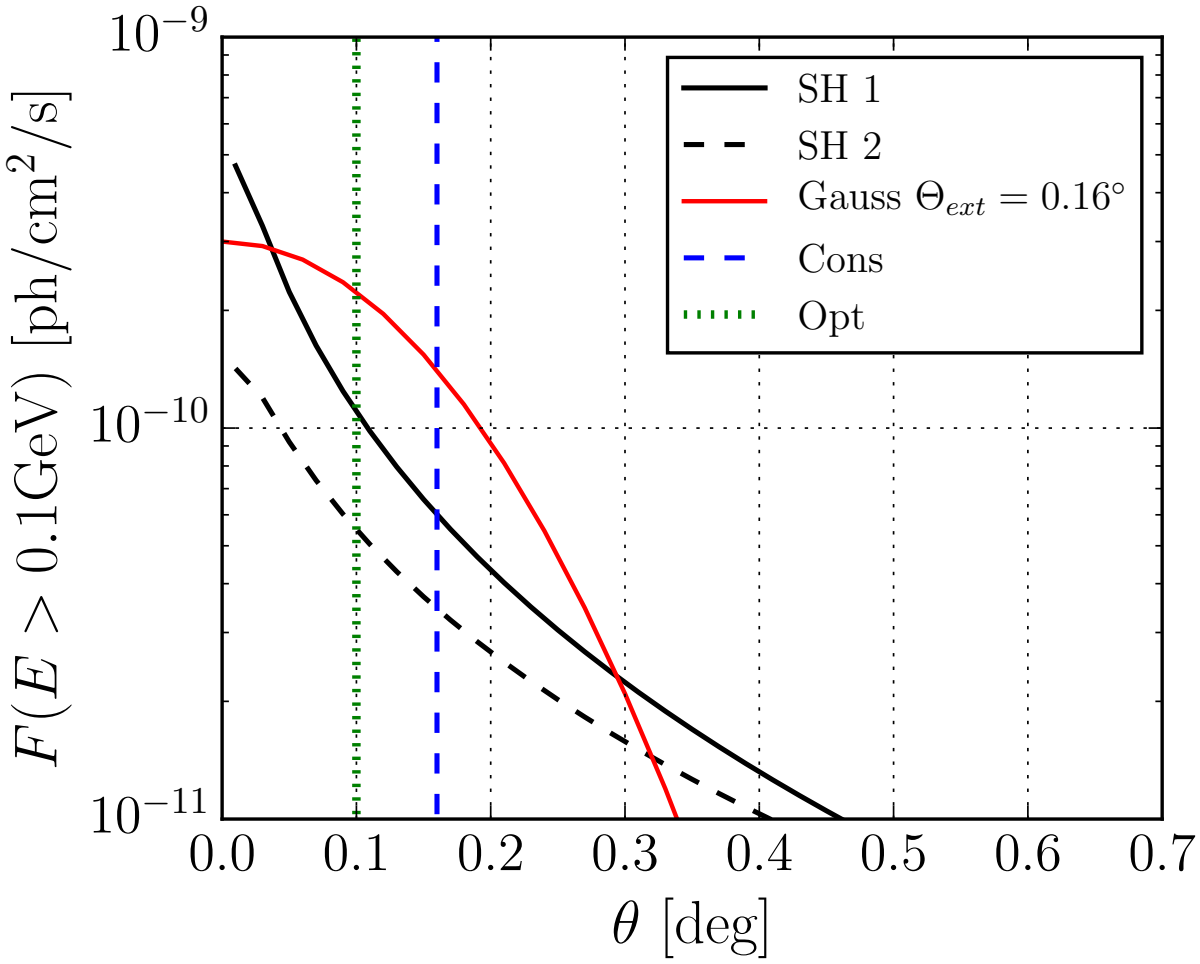

FIG. 14. Flux profile as a function of the angular separation from the center of two extended DM SHs with a flux larger than the sensitivity flux threshold of the 3FGL setup: $M_{\rm SH} = 1.9 \cdot 10^9 M_\odot$, $r_s = 1.1$ kpc and $d_{\rm SH}$ =46 kpc (solid black line), and $M_{\rm SH} = 4.7 \cdot 10^9 M_\odot$, $r_s = 1.4$ kpc and $d_{\rm SH} = 80$ kpc (dashed black line). The red solid line corresponds to a Gaussian profile with $\Theta_{\rm ext} = 0.16°$. The optimistic and conservative $\Theta_{\rm ext}$ are highlighted by the vertical green and blue line respectively.

on the dark matter annihilation cross section into gamma rays. Although the upper limits on $\langle\sigma v\rangle$ for the detection of $N_{\rm Candidate} = 5$ or 20 sub-halos are weaker than those derived with the Pass 8 analysis of dwarf galaxies [5], they become quite competitive assuming zero sub-halo candidates. For values of $\langle\sigma v\rangle$ consistent with the current limits from dwarf galaxies, we have also found that the sub-halos source count distribution is suppressed by more than three orders of magnitude with respect to the observed flux distribution of blazars in both the 3FGL and 2FHL catalogs. Moreover, we have investigated the impact of adding smaller mass sub-halos ($10^5\ M_\odot < M_{\rm SH} < 5 \times 10^6\ M_\odot$) to the sub-halo population. Their effect is to increase the number of sources per unit flux at very small fluxes. As a consequence, they have no effect on the number of detectable sub-halos and on the bounds to the annihilation cross section for current sensitivities.

One discriminating feature for the identification of dark matter sub-halos would be the spatial extension of the source. About one sub-halo of our simulated population turns out to be detectable in the 3FGL as extended source. We recall that conservative assumptions have been made in the present work. Indeed, we expect a great improvement with the new Pass 8 4FGL, which could significantly increase the number of detectable sub-halos, and possibly lead to the identification of some unassociated sources with dark matter halo substructures thanks to their spatial extent. As an illustrative example of future progresses, we have considered a gamma-ray instrument with a factor of 5 better sensitivity than the LAT above 100 MeV, an improvement that can be achieved by new concept MeV telescopes such as e-ASTROGAM [92] and Compair [91]. Given the input of the adopted simulation, we have found that it will be possible to detect a few sub-halos (about 2.1), with a probability of 75% (1.5/2.1) to detect a dwarf galaxy.

We finally also note the relentless efforts in the numerical simulations for the reliable inclusion of the effects of baryons in the formation of galactic structures. These latter research leaves room open to further inspections, once

Milky Way size halos will be realized with even greater resolution.

ACKNOWLEDGMENTS

We acknowledge fruitful discussions with G. Bertone, D. Schoonenberg, Q. Zhu, H. S. Zechlin, S. Palomares-Ruiz, E. Charles and M. Wood. We also thank V. Springel for comments on the manuscript. FC acknowledges partial support (for the initial stages of this work) from the European Research Council through the ERC starting grant WIMPs Kairos, P.I. G. Bertone. VDR acknowledges support by the Spanish MINECO through the project FPA2012-31880 (P.I. Enrique Alvarez Vazquez) and partial support from the EU's Horizon 2020 research and innovation programme under the Marie Sklodowska-Curie grant agreements No 690575 and No 674896. MDM acknowledges support by the NASA Fermi Guest Investigator Program 2014 through the Fermi multi-year Large Program N. 81303 (P.I. E. Charles). FC and FM would like to express a special thank to the Mainz Institute for Theoretical Physics (MITP) for its hospitality and support.

[1] F. Marinacci, R. Pakmor, and V. Springel, *The formation of disc galaxies in high resolution moving-mesh cosmological simulations*, *Mon. Not. Roy. Astron. Soc.* **437** (2014), no. 2 1750–1775, [arXiv:1305.5360].

[2] **Planck** Collaboration, P. A. R. Ade et al., *Planck 2015 results. XIII. Cosmological parameters*, *A&A* **594** (2016) A13, [arXiv:1502.01589].

[3] J. Silk et al., *Particle Dark Matter: Observations, Models and Searches*. 2010.

[4] G. Bertone, D. Hooper, and J. Silk, *Particle dark matter: Evidence, candidates and constraints*, *Phys. Rept.* **405** (2005) 279–390, [hep-ph/0404175].

[5] **Fermi-LAT** Collaboration, M. Ackermann et al., *Searching for Dark Matter Annihilation from Milky Way Dwarf Spheroidal Galaxies with Six Years of Fermi Large Area Telescope Data*, *Phys. Rev. Lett.* **115** (2015), no. 23 231301, [arXiv:1503.02641].

[6] C. Weniger, *A Tentative Gamma-Ray Line from Dark Matter Annihilation at the Fermi Large Area Telescope*, *JCAP* **1208** (2012) 007, [arXiv:1204.2797].

[7] **Fermi-LAT** Collaboration, M. Ackermann et al., *Search for gamma-ray spectral lines with the Fermi large area telescope and dark matter implications*, *Phys. Rev.* **D88** (2013) 082002, [arXiv:1305.5597].

[8] T. Bringmann, F. Calore, M. Di Mauro, and F. Donato, *Constraining dark matter annihilation with the isotropic γ-ray background: updated limits and future potential*, *Phys. Rev.* **D89** (2014), no. 2 023012, [arXiv:1303.3284].

[9] M. Ajello et al., *The Origin of the Extragalactic Gamma-Ray Background and Implications for Dark-Matter Annihilation*, *Astrophys. J.* **800** (2015), no. 2 L27, [arXiv:1501.05301].

[10] M. Di Mauro and F. Donato, *Composition of the Fermi-LAT isotropic gamma-ray background intensity: Emission from extragalactic point sources and dark matter annihilations*, *Phys. Rev.* **D91** (2015), no. 12 123001, [arXiv:1501.05316].

[11] **Fermi-LAT** Collaboration, M. Ackermann et al., *Search for extended gamma-ray emission from the Virgo galaxy cluster with Fermi-LAT*, *Astrophys. J.* **812** (2015), no. 2 159, [arXiv:1510.00004].

[12] F. Calore, I. Cholis, and C. Weniger, *Background model systematics for the Fermi GeV excess*, *JCAP* **1503** (2015) 038, [arXiv:1409.0042].

[13] **Fermi-LAT** Collaboration, M. Ajello et al., *Fermi-LAT Observations of High-Energy γ-Ray Emission Toward the Galactic Center*, *Astrophys. J.* **819** (2016), no. 1 44, [arXiv:1511.02938].

[14] C. L. Bennett, D. Larson, J. L. Weiland, N. Jarosik, G. Hinshaw, N. Odegard, K. M. Smith, R. S. Hill, B. Gold, M. Halpern, E. Komatsu, M. R. Nolta, L. Page, D. N. Spergel, E. Wollack, J. Dunkley, A. Kogut, M. Limon, S. S. Meyer, G. S. Tucker, and E. L. Wright, *Nine-year Wilkinson Microwave Anisotropy Probe (WMAP) Observations: Final Maps and Results*, *ApJS* **208** (Oct., 2013) 20, [arXiv:1212.5225].

[15] J. F. Navarro, C. S. Frenk, and S. D. M. White, *The Structure of Cold Dark Matter Halos*, *ApJ* **462** (May, 1996) 563, [astro-ph/9508025].

[16] J. F. Navarro, C. S. Frenk, and S. D. M. White, *A Universal Density Profile from Hierarchical Clustering*, *ApJ* **490** (Dec., 1997) 493–508, [astro-ph/9611107].

[17] S. D. M. White and C. S. Frenk, *Galaxy formation through hierarchical clustering*, *Astrophys. J.* **379** (1991) 52–79.

[18] V. Springel, S. D. M. White, A. Jenkins, C. S. Frenk, N. Yoshida, L. Gao, J. Navarro, R. Thacker, D. Croton, J. Helly, J. A. Peacock, S. Cole, P. Thomas, H. Couchman, A. Evrard, J. Colberg, and F. Pearce, *Simulations of the formation, evolution and clustering of galaxies and quasars*, *Nature* **435** (June, 2005) 629–636, [astro-ph/0504097].

[19] M. Boylan-Kolchin, V. Springel, S. D. M. White, A. Jenkins, and G. Lemson, *Resolving cosmic structure formation with the Millennium-II Simulation*, *MNRAS* **398** (Sept., 2009) 1150–1164, [arXiv:0903.3041].

[20] R. E. Angulo, V. Springel, S. D. M. White, A. Jenkins, C. M. Baugh, and C. S. Frenk, *Scaling relations for galaxy clusters in the Millennium-XXL simulation*, *MNRAS* **426** (Nov., 2012) 2046–2062, [arXiv:1203.3216].

[21] A. A. Dutton, A. V. Macciò, A. Dekel, L. Wang, G. S. Stinson, A. Obreja, A. Di Cintio, C. B. Brook, T. Buck, and X. Kang, *NIHAO IX: The role of gas inflows and outflows in driving the contraction and expansion of cold dark matter haloes*, *ArXiv e-prints* (May, 2016) [arXiv:1605.05323].

[22] A. Di Cintio, C. B. Brook, A. V. Macciò, G. S. Stinson, A. Knebe, A. A. Dutton, and J. Wadsley, *The dependence of dark matter profiles on the stellar-to-halo mass ratio: a prediction for cusps versus cores*, *MNRAS* **437** (Jan., 2014) 415–423, [arXiv:1306.0898].

[23] A. Pontzen and F. Governato, *Cold dark matter heats up*, *Nature* **506** (Feb., 2014) 171–178, [arXiv:1402.1764].

[24] M. Vogelsberger, S. Genel, V. Springel, P. Torrey, D. Sijacki, D. Xu, G. F. Snyder, S. Bird, D. Nelson, and L. Hernquist, *Properties of galaxies reproduced by a hydrodynamic simulation*, *Nature* **509** (2014) 177–182, [arXiv:1405.1418].

[25] M. Vogelsberger, S. Genel, V. Springel, P. Torrey, D. Sijacki, D. Xu, G. Snyder, D. Nelson, and L. Hernquist, *Introducing the Illustris Project: simulating the coevolution of dark and visible matter in the Universe*, *MNRAS* **444** (Oct., 2014) 1518–1547, [arXiv:1405.2921].

[26] J. Schaye, R. A. Crain, R. G. Bower, M. Furlong, M. Schaller, T. Theuns, C. Dalla Vecchia, C. S. Frenk, I. G. McCarthy, J. C. Helly, A. Jenkins, Y. M. Rosas-Guevara, S. D. M. White, M. Baes, C. M. Booth, P. Camps, J. F. Navarro, Y. Qu, A. Rahmati, T. Sawala, P. A. Thomas, and J. Trayford, *The EAGLE project: simulating the evolution and assembly of galaxies and their environments*, *MNRAS* **446** (Jan., 2015) 521–554, [arXiv:1407.7040].

[27] O. Agertz, R. Teyssier, and B. Moore, *The formation of disc galaxies in a ΛCDM universe*, *MNRAS* **410** (Jan., 2011) 1391–1408, [arXiv:1004.0005].

[28] M. Aumer, S. D. M. White, T. Naab, and C. Scannapieco, *Towards a more realistic population of bright spiral galaxies in cosmological simulations*, *MNRAS* **434** (Oct., 2013) 3142–3164, [arXiv:1304.1559].

[29] R. J. J. Grand, F. A. Gómez, F. Marinacci, R. Pakmor, V. Springel, D. J. R. Campbell, C. S. Frenk, A. Jenkins, and S. D. M. White, *The Auriga Project: the properties and formation mechanisms of disc galaxies across cosmic time*, *ArXiv e-prints* (Oct., 2016) [arXiv:1610.01159].

[30] J. Guedes, S. Callegari, P. Madau, and L. Mayer, *Forming Realistic Late-type Spirals in a ΛCDM Universe: The Eris Simulation*, *ApJ* **742** (Dec., 2011) 76, [arXiv:1103.6030].

[31] P. Mollitor, E. Nezri, and R. Teyssier, *Baryonic and dark matter distribution in cosmological simulations of spiral galaxies*, *MNRAS* **447** (Feb., 2015) 1353–1369, [arXiv:1405.4318].

[32] G. S. Stinson, C. Brook, A. V. Macciò, J. Wadsley, T. R. Quinn, and H. M. P. Couchman, *Making Galaxies In a Cosmological Context: the need for early stellar feedback*, *MNRAS* **428** (Jan., 2013) 129–140, [arXiv:1208.0002].

[33] L. Wang, A. A. Dutton, G. S. Stinson, A. V. Macciò, C. Penzo, X. Kang, B. W. Keller, and J. Wadsley, *NIHAO project - I. Reproducing the inefficiency of galaxy formation across cosmic time with a large sample of cosmological hydrodynamical simulations*, *MNRAS* **454** (Nov., 2015) 83–94, [arXiv:1503.04818].

[34] P. Colín, V. Avila-Reese, S. Roca-Fàbrega, and O. Valenzuela, *Cosmological simulations of Milky Way-sized galaxies*, *ApJ* **829** (Oct., 2016) 98, [arXiv:1607.07917].

[35] **Dark Energy Survey** Collaboration, B. Flaugher, *The Dark Energy Survey*, *Int. J. Mod. Phys.* **A20** (2005) 3121–3123.

[36] **DES, Fermi-LAT** Collaboration, A. Drlica-Wagner et al., *Search for Gamma-Ray Emission from DES Dwarf Spheroidal Galaxy Candidates with Fermi-LAT Data*, *Astrophys. J.* **809** (2015), no. 1 L4, [arXiv:1503.02632].

[37] **DES** Collaboration, K. Bechtol et al., *Eight New Milky Way Companions Discovered in First-Year Dark Energy Survey Data*, *Astrophys. J.* **807** (2015), no. 1 50, [arXiv:1503.02584].

[38] **Fermi-LAT** Collaboration, A. A. Abdo et al., *Observations of Milky Way Dwarf Spheroidal galaxies with the Fermi-LAT detector and constraints on Dark Matter models*, *Astrophys. J.* **712** (2010) 147–158, [arXiv:1001.4531].

[39] **Fermi-LAT, MAGIC** Collaboration, M. L. Ahnen et al., *Limits to dark matter annihilation cross-section from a combined analysis of MAGIC and Fermi-LAT observations of dwarf satellite galaxies*, *JCAP* **1602** (2016), no. 02 039, [arXiv:1601.06590].

[40] **Fermi-LAT** Collaboration, M. Ackermann et al., *The spectrum of isotropic diffuse gamma-ray emission between 100 MeV and 820 GeV*, *Astrophys. J.* **799** (2015) 86, [arXiv:1410.3696].

[41] V. Springel, S. D. M. White, C. S. Frenk, J. F. Navarro, A. Jenkins, M. Vogelsberger, J. Wang, A. Ludlow, and A. Helmi, *Prospects for detecting supersymmetric dark matter in the Galactic halo*, *Nature* **456** (Nov., 2008) 73–76, [arXiv:0809.0894].

[42] **Fermi-LAT** Collaboration, M. Ackermann et al., *Limits on Dark Matter Annihilation Signals from the Fermi LAT 4-year Measurement of the Isotropic Gamma-Ray Background*, *JCAP* **1509** (2015), no. 09 008, [arXiv:1501.05464].

[43] F. Calore, V. De Romeri, M. Di Mauro, F. Donato, J. Herpich, A. V. Macciò, and L. Maccione, *γ-ray anisotropies from dark matter in the Milky Way: the role of the radial distribution*, *Mon. Not. Roy. Astron. Soc.* **442** (2014), no. 2 1151–1156, [arXiv:1402.0512].

[44] M. Fornasa et al., *Angular power spectrum of the diffuse gamma-ray emission as measured by the Fermi Large Area Telescope and constraints on its dark matter interpretation*, *Phys. Rev.* **D94** (2016), no. 12 123005, [arXiv:1608.07289].

[45] F. Acero et al., *Fermi Large Area Telescope Third Source Catalog*, *Astrophys. J. Suppl.* **218** (2015), no. 2 23.

[46] **Fermi-LAT** Collaboration, W. Atwood et al., *Pass 8: Toward the Full Realization of the Fermi-LAT Scientific Potential*, 2013. arXiv:1303.3514.

[47] **Fermi-LAT** Collaboration, M. Ackermann et al., *2FHL: The Second Catalog of Hard Fermi-LAT Sources*, *Astrophys. J. Suppl.* **222** (2016), no. 1 5, [arXiv:1508.04449].

[48] B. Bertoni, D. Hooper, and T. Linden, *Examining The Fermi-LAT Third Source Catalog In Search Of Dark Matter Subhalos*, *JCAP* **1512** (2015), no. 12 035, [arXiv:1504.02087].

[49] B. Bertoni, D. Hooper, and T. Linden, *Is The Gamma-Ray Source 3FGL J2212.5+0703 A Dark Matter Subhalo?*, *JCAP* **1605** (2016) 049, [arXiv:1602.07303].

[50] D. Schoonenberg, J. Gaskins, G. Bertone, and J. Diemand, *Dark matter subhalos and unidentified sources in the Fermi 3FGL source catalog*, *JCAP* **1605** (2016), no. 05 028, [arXiv:1601.06781].

[51] D. Hooper and S. J. Witte, *Gamma Rays From Dark Matter Subhalos Revisited: Refining the Predictions and Constraints*, *JCAP* **1704** (2017), no. 04 018, [arXiv:1610.07587].

[52] J. Diemand, M. Kuhlen, P. Madau, M. Zemp, B. Moore, D. Potter, and J. Stadel, *Clumps and streams in the local dark matter distribution*, *Nature* **454** (2008) 735–738, [arXiv:0805.1244].

[53] M. Htten, C. Combet, G. Maier, and D. Maurin, *Dark matter substructure modelling and sensitivity of the Cherenkov Telescope Array to Galactic dark halos*, *JCAP* **1609** (2016), no. 09 047, [arXiv:1606.04898].

[54] B. S. Acharya et al., *Introducing the CTA concept*, *Astropart. Phys.* **43** (2013) 3–18.

[55] N. Mirabal, E. Charles, E. C. Ferrara, P. L. Gonthier, A. K. Harding, M. A. Snchez-Conde, and D. J. Thompson, *3FGL Demographics Outside the Galactic Plane using Supervised Machine Learning: Pulsar and Dark Matter Subhalo Interpretations*, *Astrophys. J.* **825** (2016), no. 1 69, [arXiv:1605.00711].

[56] S. Garrison-Kimmel, M. Boylan-Kolchin, J. Bullock, and K. Lee, *ELVIS: Exploring the Local Volume in Simulations*, *Mon. Not. Roy. Astron. Soc.* **438** (2014), no. 3 2578–2596, [arXiv:1310.6746].

[57] Q. Zhu, F. Marinacci, M. Maji, Y. Li, V. Springel, and L. Hernquist, *Baryonic impact on the dark matter distribution in Milky Way-sized galaxies and their satellites*, *Mon. Not. Roy. Astron. Soc.* **458** (2016), no. 2 1559–1580, [arXiv:1506.05537].

[58] E. Sefusatti, G. Zaharijas, P. D. Serpico, D. Theurel, and M. Gustafsson, *Extragalactic gamma-ray signal from dark matter annihilation: an appraisal*, *Mon. Not. Roy. Astron. Soc.* **441** (2014), no. 3 1861–1878, [arXiv:1401.2117].

[59] M. Di Mauro, F. Calore, F. Donato, M. Ajello, and L. Latronico, *Diffuse γ-ray emission from misaligned active galactic nuclei*, *Astrophys. J.* **780** (2014) 161, [arXiv:1304.0908].

[60] M. Di Mauro, F. Donato, G. Lamanna, D. A. Sanchez, and P. D. Serpico, *Diffuse γ-ray emission from unresolved BL Lac objects*, *Astrophys. J.* **786** (2014) 129, [arXiv:1311.5708].

[61] V. Springel, J. Wang, M. Vogelsberger, A. Ludlow, A. Jenkins, A. Helmi, J. F. Navarro, C. S. Frenk, and S. D. M. White, *The Aquarius Project: the subhaloes of galactic haloes*, *MNRAS* **391** (2008) 1685–1711.

[62] V. Springel and L. Hernquist, *Cosmological smoothed particle hydrodynamics simulations: a hybrid multiphase model for star formation*, *MNRAS* **339** (Feb., 2003) 289–311, [astro-ph/0206393].

[63] G. Chabrier, *The Galactic Disk Mass Function: Reconciliation of the Hubble Space Telescope and Nearby Determinations*, *ApJL* **586** (Apr., 2003) L133–L136, [astro-ph/0302511].

[64] M. Vogelsberger, S. Genel, D. Sijacki, P. Torrey, V. Springel, and L. Hernquist, *A model for cosmological simulations of galaxy formation physics*, *MNRAS* **436** (Dec., 2013) 3031–3067, [arXiv:1305.2913].

[65] V. Springel, *E pur si muove: Galilean-invariant cosmological hydrodynamical simulations on a moving mesh*, *MNRAS* **401** (Jan., 2010) 791–851, [arXiv:0901.4107].

[66] J. P. Ostriker, L. Spitzer, Jr., and R. A. Chevalier, *On the Evolution of Globular Clusters*, *ApJL* **176** (Sept., 1972) L51.

[67] E. D'Onghia, V. Springel, L. Hernquist, and D. Keres, *Substructure Depletion in the Milky Way Halo by the Disk*, *ApJ* **709** (Feb., 2010) 1138–1147, [arXiv:0907.3482].

[68] G. R. Blumenthal, S. M. Faber, R. Flores, and J. R. Primack, *Contraction of dark matter galactic halos due to baryonic infall*, *ApJ* **301** (Feb., 1986) 27–34.

[69] O. Y. Gnedin, A. V. Kravtsov, A. A. Klypin, and D. Nagai, *Response of Dark Matter Halos to Condensation of Baryons: Cosmological Simulations and Improved Adiabatic Contraction Model*, *ApJ* **616** (Nov., 2004) 16–26, [astro-ph/0406247].

[70] M. Zemp, O. Y. Gnedin, N. Y. Gnedin, and A. V. Kravtsov, *The Impact of Baryon Physics on the Structure of High-redshift Galaxies*, *ApJ* **748** (Mar., 2012) 54, [arXiv:1108.5384].

[71] E. D'Onghia, G. Besla, T. J. Cox, and L. Hernquist, *Resonant stripping as the origin of dwarf spheroidal galaxies*, *Nature* **460** (July, 2009) 605–607, [arXiv:0907.2442].

[72] D. Yurin and V. Springel, *The stability of stellar disks in Milky-Way sized dark matter halos*, *Mon. Not. Roy. Astron. Soc.* **452** (2015) 2343, [arXiv:1411.3729].

[73] S. P. D. Gill, A. Knebe, and B. K. Gibson, *The evolution of substructure - I. A new identification method*, *MNRAS* **351** (June, 2004) 399–409, [astro-ph/0404258].

[74] S. R. Knollmann and A. Knebe, *AHF: Amiga's Halo Finder*, *ApJS* **182** (June, 2009) 608–624, [arXiv:0904.3662].

[75] L. Gao, J. F. Navarro, C. S. Frenk, A. Jenkins, V. Springel, and S. D. M. White, *The Phoenix Project: the Dark Side of Rich Galaxy Clusters*, *Mon. Not. Roy. Astron. Soc.* **425** (2012) 2169, [arXiv:1201.1940].

[76] M. Schaller et al., *Dark matter annihilation radiation in hydrodynamic simulations of Milky Way haloes*, *Mon. Not. Roy. Astron. Soc.* **455** (2016), no. 4 4442–4451, [arXiv:1509.02166].

[77] F. Calore, N. Bozorgnia, M. Lovell, G. Bertone, M. Schaller, C. S. Frenk, R. A. Crain, J. Schaye, T. Theuns, and J. W. Trayford, *Simulated Milky Way analogues: implications for dark matter indirect searches*, *JCAP* **1512** (2015), no. 12 053, [arXiv:1509.02164].

[78] J. Oñorbe, M. Boylan-Kolchin, J. S. Bullock, P. F. Hopkins, D. Kereš, C.-A. Faucher-Giguère, E. Quataert, and N. Murray, *Forged in FIRE: cusps, cores and baryons in low-mass dwarf galaxies*, *MNRAS* **454** (Dec., 2015) 2092–2106, [arXiv:1502.02036].

[79] T. Sawala, C. S. Frenk, A. Fattahi, J. F. Navarro, R. G. Bower, R. A. Crain, C. Dalla Vecchia, M. Furlong, J. C. Helly, A. Jenkins, K. A. Oman, M. Schaller, J. Schaye, T. Theuns, J. Trayford, and S. D. M. White, *The APOSTLE simulations: solutions to the Local Group's cosmic puzzles*, *MNRAS* **457** (Apr., 2016) 1931–1943, [arXiv:1511.01098].

[80] F. Governato, A. Zolotov, A. Pontzen, C. Christensen, S. H. Oh, A. M. Brooks, T. Quinn, S. Shen, and J. Wadsley, *Cuspy no more: how outflows affect the central dark matter and baryon distribution in Λ cold dark matter galaxies*, *MNRAS* **422** (May, 2012) 1231–1240, [arXiv:1202.0554].

[81] J. Einasto and U. Haud, *Galactic models with massive corona. I - Method. II - Galaxy*, *A&A* **223** (Oct., 1989) 89–106.

[82] L. Pieri, J. Lavalle, G. Bertone, and E. Branchini, *Implications of High-Resolution Simulations on Indirect Dark Matter Searches*, *Phys. Rev.* **D83** (2011) 023518, [arXiv:0908.0195].

[83] Sánchez-Conde, Miguel A. and Prada, Francisco, *The flattening of the concentration-mass relation towards low halo masses and its implications for the annihilation signal boost*, *Mon. Not. Roy. Astron. Soc.* **442** (2014), no. 3 2271–2277, [arXiv:1312.1729].

[84] R. Bartels and S. Ando, *Boosting the annihilation boost: Tidal effects on dark matter subhalos and consistent luminosity modeling*, *Phys. Rev.* **D92** (2015), no. 12 123508, [arXiv:1507.08656].

[85] . Molin, M. A. Snchez-Conde, S. Palomares-Ruiz, and F. Prada, *Characterization of subhalo structural properties and implications for dark matter annihilation signals*, *Mon. Not. Roy. Astron. Soc.* **466** (2017), no. 4 4974–4990, [arXiv:1603.04057].

[86] S. Ghigna, B. Moore, F. Governato, G. Lake, T. Quinn, and J. Stadel, *Density Profiles and Substructure of Dark Matter Halos: Converging Results at Ultra-High Numerical Resolution*, *ApJ* **544** (Dec., 2000) 616–628, [astro-ph/9910166].

[87] M. Cirelli, G. Corcella, A. Hektor, G. Hutsi, M. Kadastik, P. Panci, M. Raidal, F. Sala, and A. Strumia, *PPPC 4 DM ID: A Poor Particle Physicist Cookbook for Dark Matter Indirect Detection*, *JCAP* **1103** (2011) 051, [arXiv:1012.4515]. [Erratum: JCAP1210,E01(2012)].

[88] Sjöstrand, Torbjörn and Ask, Stefan and Christiansen, Jesper R. and Corke, Richard and Desai, Nishita and Ilten, Philip and Mrenna, Stephen and Prestel, Stefan and Rasmussen, Christine O. and Skands, Peter Z., *An Introduction to PYTHIA 8.2*, *Comput. Phys. Commun.* **191** (2015) 159–177, [arXiv:1410.3012].

[89] A. Burkert, *The Structure of Dark Matter Halos in Dwarf Galaxies*, *ApJL* **447** (July, 1995) L25–L28, [astro-ph/9504041].

[90] **Fermi-LAT** Collaboration, *The Fermi-LAT high-latitude Survey: Source Count Distributions and the Origin of the Extragalactic Diffuse Background*, *Astrophys. J.* **720** (2010) 435–453, [arXiv:1003.0895].

[91] A. A. Moiseev et al., *Compton-Pair Production Space Telescope (ComPair) for MeV Gamma-ray Astronomy*, arXiv:1508.07349.

[92] **on behalf of the e-ASTROGAM** Collaboration, A. De Angelis et al., *The e-ASTROGAM mission (exploring the extreme Universe in the MeV-GeV range)*, arXiv:1611.02232.

[93] **Fermi-LAT** Collaboration, M. Ackermann et al., *Resolving the Extragalactic γ-ray Background above 50 GeV with Fermi-LAT*, *Phys. Rev. Lett.* **116** (2016), no. 15 151105, [arXiv:1511.00693].